LA-UR-21-22866
Approved for public release; distribution is unlimited.

Title: QED with the electron as a very small black-hole-like object

Author(s): Lestone, John Paul

Intended for: Web

Issued: 2021-03-24

LA-UR-21-xxxxx

QED with the electron as a very small black-hole-like object

J. P. Lestone
Computational Physics Division, Los Alamos National Laboratory
Los Alamos, NM 87545, USA
February 21st, 2021

Abstract

We pursue a simple semi-classical particle-based picture of QED in which the electron is assumed to contain a point massless and chargeless core that interacts with the electromagnetic vacuum in ways that are not dissimilar to the manner in which small black holes may interact with photons. Modifications are made to obtain known properties of the electron including the presence of rest energy, Lamb shift, magnetic moments (both free and bound), charge, Larmor emission, and vacuum polarization. The present study does not provide proofs but is rather an attempt to reverse-engineer the photon-electron and black-hole-electron interaction properties needed to match experimental observations. The ease by which many QED observables can be reproduced suggests further study of the presented framework may be warranted. Future detailed analysis of the exchange of long wavelength Hawking radiation between a pair of small black holes will be of particular interest.

I. Introduction

Particle physics is viewed through the lens of quantum electrodynamics [1,2,3] (QED) and subsequent developments in quantum field theories which have led to the highly successful standard model. Despite our detailed understanding of particle physics, numerous long-standing mysteries remain. These include a reason for the existence of three generations of leptons and quarks; the corresponding fundamental unit of charge, $e = 1.602176634\times10^{-19}$ C [4], as expressed by the charged leptons; and the one-third and two-thirds fractional charges expressed by the quarks. Here, we use a simple semi-classical particle-based framework to attack the mystery of the existence of the fundamental unit of charge. At the core of this problem is the fine-structure constant, α, which controls the strength of the photon-electron interaction in QED. This central electromagnetic constant is, for standard QED, an inputted model parameter obtained by experiment, $\alpha = 1/137.035999206(11)$ [5]. For this number to be a theoretically calculable value, QED must be an approximation of a more fundamental theory.

There have been many attempts to understand the numerical value of the fine-structure constant [6]. We believe it is logical that one needs to study a mechanism by which point-like non-charged particles can interact with the electromagnetic field, if one hopes to create a successful theory to explain why charge exists and why it has a fundamental unit. If such a mechanism existed, it might then be possible to infer various outcomes associated with this interaction. If any of the calculated outcomes have similarities with electromagnetism, then this would be a window into a possible calculation of the properties of charged particles not available via standard electromagnetic theory. The only simple mechanism that we are aware of where a point-like chargeless particle can interact with photons is the interaction of photons with black holes [7]. The idea of black holes as elementary particles is not new [8,9,10]. However, here we take the view that because black holes are objects amenable to statistical analysis, then elementary particles may

also be representable by a statistical picture and capable of particle evaporation. We have previously explored the possibility that photon exchanges (evaporation and absorption) between black holes might be related to charge [11]. The repulsive force between two identical black holes due to the classical exchange of their Hawking radiation can be used to define an effective charge of $\sim 10^{-19}$ C [11]. Despite serious issues with the classical Hawking-radiation-exchange concept, the proximity of the inferred charge to the fundamental unit of charge suggested further study was warranted. Here we expand the classical Hawking-radiation-exchange concept into a more quantum-like exchange which assumes electrons contain a massless and intrinsically chargeless point particle that interacts with the electromagnetic vacuum. The present work cannot be used to prove that elementary charged particles are small black holes. However, we can show that if point-like chargeless particles interact with photons in a way that is not dissimilar to the manner in which small chargeless black holes are expected to interact with photons, then several properties that give the appearance of a charged particle can be obtained. Given these comments, it is important to review the nature of black hole photon interactions (see section II).

There is no accepted theory of the properties of small black holes with masses in the range of subatomic particles. Therefore, we cannot provide an analysis based on a well-established theory. We instead search for photon-electron and black-hole-electron interaction properties, inspired by the possible properties of micro black holes, which give the known properties of the electron. To do this we start with the properties of the electron known to us via QED. Standard QED is a quantum field theory that starts with fields and can be used to infer particle properties and interaction cross sections. We attempt to turn this the other way around and desire a particle-based picture with well-defined interaction cross sections that can be used to infer the properties of fields. In effect, we assume that there exists a black hole particle-based picture of quantum-electro-dynamics that is equivalent or nearly identical to the standard field-based approach known as QED. We then use this assumed near equivalence to infer the properties of small black holes. Therefore, in many instances in this paper it may appear that I make unsubstantiated claims about the properties of small black holes (and/or electron-photon and black-hole-electron interactions), but please interpret these as suggestions and read on to see that these claims are made because, within the framework of a semi-classical particle-based picture, they give outcomes that are the same as, or very similar to, that from standard QED.

In section III we show an equivalence between the rate of $L = 0$ real photon emission from a black body and the emission rate of $L = 0$ virtual photons from a small black hole. In section IV we show that these virtual emissions form a cloud surrounding each black hole and can be used to construct a description of the rest-mass energy and inertia of particles. In this picture, the properties of particles are not controlled by a charge and/or mass assigned to charged particles, but instead emerge due to the way the massless and chargeless particles (small black holes) interact with the electromagnetic vacuum state. By allowing some fraction of virtual-photon black-hole interactions to introduce particle recoils, a simple description of the Lamb shift is obtained in section V. These particle recoils allow for a simple semi-classical method by which point-particles can self-interact. The properties of this self-interaction are tuned in section VI to obtain a description of the magnetic moment of electrons (both free and bound). The self-interaction mechanism enables the exchange of virtual photons between a particle pair. The exchanging photons have thermal properties with an effective temperature controlled by the distance between the exchanging particles. This exchange, in turn, generates a force (see section VII) that can be used to define a fundamental unit of charge that is close to the known value from experiment, and can be used to obtain a new picture of Larmor emission from accelerating charged particles (see section VIII). In section IX we explore a new picture of vacuum polarization by expanding the photon-exchange mechanism mentioned above to include the exchange of virtual electrons (black holes) and correlated electron clusters between a real particle pair. These exchanges are also driven by a thermal-like evaporation process. The radial

dependence of the interaction potential, in this new model, is very close to that from vacuum polarization over ten orders of magnitude in relative potential change, across four orders of magnitude in distance down to length scales as small as one thousandth of a reduced Compton wavelength. Additional work is needed to confirm or negate the presented suggestions. We hope that the inferred virtual-photon particle interactions and virtual black hole particle interaction properties used here might illuminate the way forward to a new more complete theory.

II. Emission and absorption of photons by black holes

The emission and absorption of real photons by a Schwarzschild black hole (with mass M and radius r_S) is well understood [7,12,13,14] and controlled by an energy and angular momentum dependent absorption cross section [14]

$$\sigma_a(M\omega) = \sum_{L=1}^{\infty} \frac{(2L+1)\pi r_S^2}{4(M\omega)^2} T_L(M\omega) = \sum_{L=1}^{\infty} T_L(\lambda\!\!\!^{-})(2L+1)\pi\lambda\!\!\!^{-2}\,, \tag{1}$$

where the T_L are transmission coefficients, which depend on both the angular momentum quantum number L, and the angular frequency of the photon ω. $M\omega$ can be converted into photon energy relative to the black hole's temperature by multiplying by 8π, i.e. $\varepsilon/T_{bh} = 8\pi M\omega$, where $T_{bh} = \hbar c/4\pi r_S$ is the black hole's temperature, and ε is the photon's energy with a reduced wavelength $\lambda\!\!\!^{-} = \hbar c/\varepsilon$. $L=0$ absorption is not allowed for photons incoming from infinity [see summation from $L=1$ to ∞ in Eq. (1)], and likewise due to the connection between emission and absorption (via time-reversal symmetry), $L=0$ emission to infinity is also forbidden. The transmission coefficients can be obtained by mapping the radial coordinate to the Wheeler coordinate $x = r + 2M\cdot\ln(r/2M - 1)$, and solving the wave equation [14]

$$(\omega^2 - V)[r\varphi_{\omega l}(x)] + \frac{d^2}{dx^2}[r\varphi_{\omega l}(x)] = 0 \tag{2}$$

using an effective potential

$$V = \left(1 - \frac{2M}{r}\right)\frac{L(L+1)}{r^2}\,. \tag{3}$$

The behavior of the T_L is relatively easy to understand given that in geometrical optics a photon impact parameter of $(27/4)^{1/2}\cdot r_S \sim 2.6\cdot r_S \sim 5.2M$ (in units with $c=G=1$) marks the transition from absorption to scattering, and therefore the T_L are small for $M\omega < L/5.2 \sim 0.2L$, i.e. $\varepsilon < 5L\cdot T_{bh}$ (see Fig. 1). Above this photon energy the T_L rise to approach unity at $M\omega \sim 0.2(L+1)$ as the T_L for the next partial wave start to increase significantly above zero (see Fig. 1) We have independently confirmed the results of Crispino et al [14], and found that for scoping calculations it is acceptable to approximate black hole T_L by

$$T_L(\omega) \sim \frac{1}{1 + \dfrac{\exp[(A_L - M\omega)/\delta_L]}{(M\omega)^4}}\,, \tag{4}$$

with the $A_{L=1\text{ to }5} = -0.0802$, 0.3288, 0.5990, 0.8343, and 1.0546, respectively; and the $\delta_{L=1\text{ to }5} = 0.0602$, 0.0418, 0.0367, 0.0353, and 0.0348, respectively. The corresponding T_L and σ_a are displayed in Fig. 1 and Fig. 2. Given the $1/\omega^2$ falloff in the $\sigma_a(L)$ once the T_L flatten off above $M\omega \sim 0.2(L+1)$, the absorption cross section for each partial wave peaks at $M\omega \sim 0.2(L+1/2)$ (see Fig. 2).

As pointed out by Crispino et al, the total absorption cross section (summing over all partial waves), at the high frequencies, oscillates about the geometrical optics value of $\sigma_0 = 6.75\pi r_S^2 = 27\pi M^2$ (in Planck

units). Our results displayed in Fig. 2 are indistinguishable from those in figures 1 and 2 in Crispino et al [14]. Given the ratio of the total $\sigma_a(\omega)$ to σ_0 (see Fig. 2), it is straightforward to calculate the "real" photon emission power from a macroscopic black hole ($M >>$ Planck mass, M_P) via

$$P(\varepsilon)d\varepsilon = \frac{27\pi r_S^2}{4\pi^2\hbar^3c^2}\frac{\sigma_a(\varepsilon)}{\sigma_0}\frac{\varepsilon^3 d\varepsilon}{\exp(\varepsilon/T)-1}. \quad (5)$$

To enable a direct comparison to a previous calculation of Page [13] we choose a black hole mass of $M = 5\times10^{11}$ kg and get a photon emission power of

$$P(M = 5\times10^{11}\text{ kg}, \varepsilon) \sim 7.38\times10^{12}\ \frac{\text{ergs}}{s\cdot(100\text{ MeV})}\frac{\sigma_a(\varepsilon)}{\sigma_0}\frac{(\varepsilon/\text{MeV})^3}{\exp(\varepsilon/T)-1}. \quad (6)$$

The corresponding power spectrum, using the $\sigma_a(\omega)/\sigma_0$ obtained from Fig. 2 is displayed in Fig. 3, and can be compared directly to the corresponding numerical calculation shown in Fig. 1 of Page [13]. The agreement between our calculation and that of Page, demonstrates that the calculation of the photon emission from an isolated macroscopic black hole is relatively straightforward, and was well established soon after the initial discovery of Hawking [7].

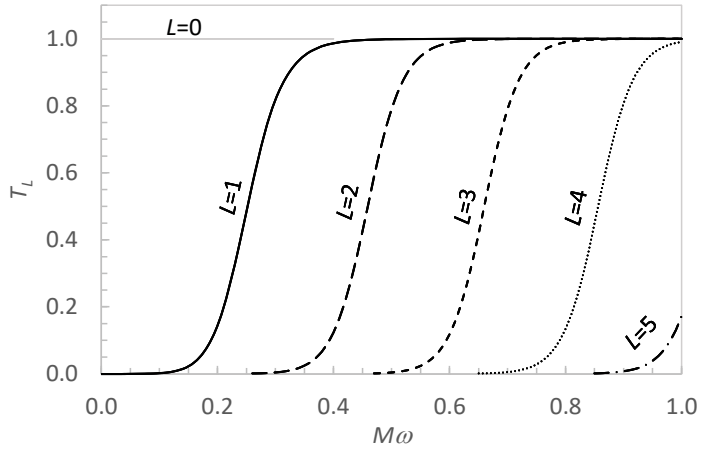

Fig. 1. Black hole transmission coefficients, T_L, versus photon frequency (see text).

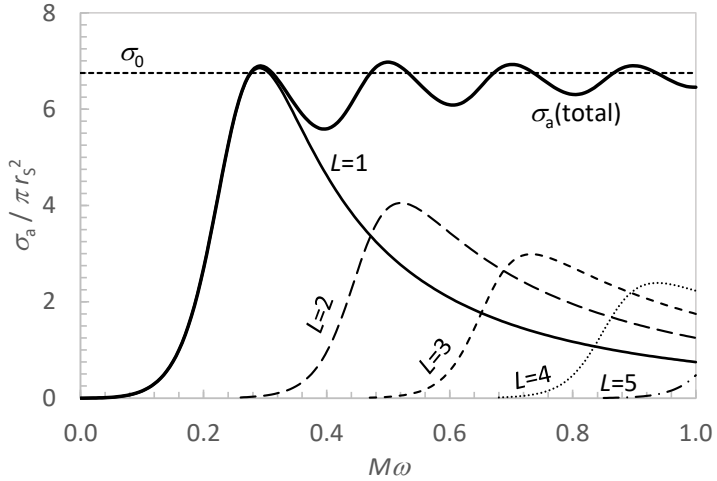

Fig. 2. Black hole total and partial-wave photon-absorption cross sections, σ_a, versus photon frequency (see text). The geometrical optics value of $\sigma_0 = 6.75\pi r_S^2$ is displayed by the horizontal dashed line.

In the limit of a zero-mass black hole (with an infinite temperature) the transition to non-zero transmission coefficients, at photon energies above $\varepsilon \sim 5L\cdot T_{bh}$, moves to inconceivably high energies for

the $L \neq 0$ partial waves, and thus the corresponding transmission coefficients are zero for all conceivable energies. However, the transmission coefficients for the unphysical $L=0$ emission stay at unity. One might therefore conclude that zero-mass black holes cannot interact with the electromagnetic field. However, in this paper we assume massless chargeless point particles can emit $L=0$ photons as long as they are later self-absorbed or reabsorbed by another particle (see section VII). With $L=0$ transmission coefficients equal to unity, as per Eq.s (2) and (3), the relevant interaction cross section is $\sigma = \pi\lambda\!\!\!^{-2}$. In this way, for small black holes, the relevant length scale is not the vanishingly small Schwarzschild radius, but instead the reduced wavelength of the $L=0$ interacting photons. This is analogous to neutron-nucleus interactions where, for fast neutrons, the relevant interaction length scale is dominated by the geometrical size of the nucleus, while for thermal neutron energies the interaction length scale is set by the reduced wavelength of the $L=0$ incident neutrons. This has profound implications for our understanding of small black holes, and will be expanded upon in following sections.

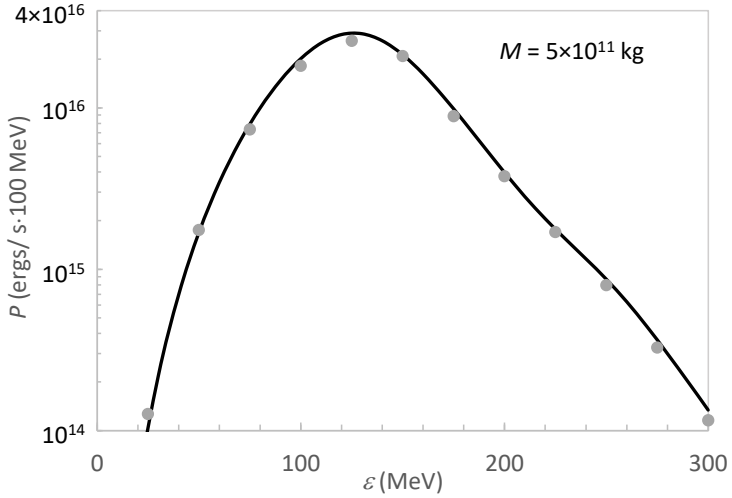

Fig. 3. Photon power spectrum from a $M = 5\times10^{11}$ kg black hole versus photon energy, ε (black curve: present results; gray circles: points read from Fig. 1 in the 1976 paper of Page [13]). The units have been chosen to facilitate a reader's own direct comparison to Page.

Another expected property of the interaction of light with black holes is stimulated emission [15]. Bekenstein and Meisels [15] have demonstrated strong similarities between the stimulated emission from atoms and black holes, with both having a probability $f = \exp(-\varepsilon/T)$ of generating a stimulated emission following the associated interaction. The only significant difference appears to be that in the atomic case the stimulated emission travels along with the corresponding exiting stimulating photon, while in the black hole case the stimulated emission travels back along the path of the incident absorbed photon. In the limit of low-energy absorption on a small high-temperature black hole the stimulated-emission probability becomes unity. This emission process in conjunction with the $L=0$ emission and self-absorption discussed in the previous paragraph, lends itself to the possibility that small black holes are surrounded by a cloud of virtual $L=0$ photons. If electrons are assumed to have some of the properties of very small black holes then perhaps the surrounding cloud of virtual photons is related to the electron's surrounding electromagnetic field; recoils associated with the absorption and emission of virtual photons could be associated with the Lamb shift; and the exchange of virtual photons between a pair of point-like chargeless objects might be the reason for the electrostatic force between electrons. These possibilities suggest a connection between quantum mechanics and black holes, and are expanded on in the following sections.

III. $L=0$ virtual-photon emission rate from a very small black hole

The spontaneous photon emission rate from a black body can be obtained via transition state theory and, in the case of a spherical black body, be expressed as [16]

$$R = 2 \times \frac{1}{h} \int_0^{\varepsilon_H} \sum_{L=0}^{\infty} (2L+1)\, T_L(\varepsilon) \exp(-\varepsilon/T)\, d\varepsilon. \tag{7}$$

The factor of two is to include both photon helicity (polarization) states. For macroscopic black bodies with a finite temperature, the high-energy cutoff, ε_H, is set to infinity, while for small black holes we will see in the next section that a finite cutoff is needed to give a finite total particle mass. We define a very small black hole to be one where the energy stored within the event horizon is infinitesimally small compared to that of the electron's rest mass. This smallness makes all the $L\neq 0$ transmission coefficients zero for the relevant photon emission energy range, $\varepsilon < \varepsilon_H$, leaving only the $L=0$ unphysical emissions (as discussed in the previous section), and a black hole temperature very large compared to ε_H. The corresponding very small black hole photon-emission rate is

$$R = \frac{1}{\pi\hbar} \int_0^{\varepsilon_H} d\varepsilon = \frac{\varepsilon_H}{\pi\hbar}. \tag{8}$$

As mentioned in the previous section, there are reasons why the emission represented by Eq. (8) cannot make it to infinity (i.e. cannot escape from an isolated particle). Some of these reasons can be partially satisfied by assuming that the $L=0$ photon emission is only allowed to exist for a timescale of $\hbar/2\varepsilon$ set by the time-energy uncertainty principle before self-absorption in the case of an isolated black hole; or before completing an exchange in the case of a black hole pair separated by a finite distance. We assume that the timescale of $\hbar/2\varepsilon$ defines a fixed probability per unit time for the "disappearance" (self-absorption) of the outwardly going $L=0$ virtual photon.

To better understand Eq. (8) it is helpful to realize that all spontaneous emission processes can be viewed as emission stimulated by vacuum-virtual photons. The rate that vacuum-virtual photons interact with an isolated point particle can be obtained by multiplying the interaction cross section, $\pi\lambda\!\!\!^{-2}$, by the number density of vacuum-virtual photons, $\varepsilon^2 d\varepsilon/\pi^2\hbar^3c^3$ [17], by the speed of light, c, giving

$$R = \int_0^{\varepsilon_H} R(\varepsilon) d\varepsilon = \int_0^{\varepsilon_H} \pi\lambda\!\!\!^{-2} \frac{\varepsilon^2 d\varepsilon}{\pi^2\hbar^3c^3} c = \int_0^{\varepsilon_H} \frac{d\varepsilon}{\pi\hbar} = \frac{\varepsilon_H}{\pi\hbar}, \tag{9}$$

in agreement with Eq. (8). Therefore, if each interaction of an $L=0$ vacuum-virtual photon is assumed to stimulate the emission of an additional virtual photon as depicted in Fig. 4 (and later in Fig. 5) then the photon emission rate is as given by Eq.s (8) and (9). This partially justifies the suggestion presented here that the black hole stimulated emission process of Bekenstein and Meisels enables $L=0$ vacuum-virtual photons to stimulate small black holes to emitted additional $L=0$ stimulated-virtual photons with a production cross section of $\pi\lambda\!\!\!^{-2}$, with an emission rate that is equivalent to the emission rate of $L=0$ photons from a black body. As already discussed, these stimulated-virtual photons cannot be allowed to escape from an isolated single particle. In the case of a small point-particle with a mass very much less than ε_H, the above introduced stimulated emission will violate conservation of energy and would not be allowed if only classical physics is assumed. However, as discussed above, we assume that the time-energy uncertainty principle allows the stimulated emission to exist for a timescale of $\tau = \hbar/2\varepsilon$, before disappearing (in a semi-classical sense). We assume a stimulated-virtual photon generated by a particle's interaction with an incident $L=0$ vacuum-virtual photon is emitted anti-parallel to the incident photon as depicted in Fig. 4 (and discussed in the previous section).

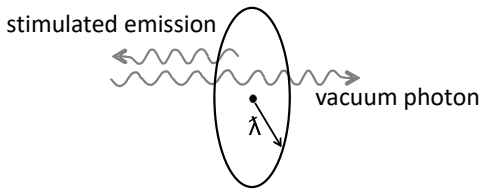

Fig. 4. Depiction of a stimulated-virtual-photon emission generated by the passage of a vacuum-virtual photon within ƛ of a small black hole (point particle). The wavelength of the schematic photons is not to scale.

IV. Rest-mass energy of very small black holes

Combining Eq. (9) with the stimulated-virtual-photon "disappearance" timescale of $\hbar/2\varepsilon$, gives the additional average virtual-photon energy (above the virtual-photon vacuum ground-state energy) associated with the presence of an isolated very small black hole as

$$\bar{E} = \int_0^{\varepsilon_H} \int_0^{\infty} \frac{\varepsilon \cdot t \exp(-2\varepsilon t/\hbar)\, dt}{\int_0^{\infty} \exp(-2\varepsilon t/\hbar)\, dt} \frac{d\varepsilon}{\pi\hbar}$$
$$= \int_0^{\varepsilon_H} \int_0^{\infty} \frac{2\varepsilon^2}{\pi\hbar^2} t \exp\left(-\frac{2\varepsilon t}{\hbar}\right) dt\, d\varepsilon = \frac{1}{2\pi}\int_0^{\varepsilon_H} d\varepsilon = \frac{\varepsilon_H}{2\pi} = mc^2. \quad (10)$$

The final step is obtained by setting the high-energy cutoff to $\varepsilon_H = 2\pi mc^2$. There are effectively three possible choices for ε_H. A value of zero would give the result that small black holes do not interact with photons. We reject this possibility for the sole reason that the outcomes would be boring. An infinite cutoff energy is rejected because it gives the unphysical result of an infinite particle energy. This leaves a finite cutoff energy as the only interesting choice, and we here choose $\varepsilon_H = 2\pi mc^2$ because it generates the result of $E = mc^2$ given at the end of Eq. (10). Here the mass m is not the mass of the small black hole being stimulated to emit, but rather the average energy in its surrounding cloud of stimulated-virtual photons divided by c^2. We will soon explore the possibility that electrons contain a massless chargeless point particle surrounded by a cloud of stimulated-virtual photons. In this case, the electron's mass is not directly related to the mass of the central point particle but is instead set by the average energy in the surrounding cloud, controlled by the high-energy cutoff, ε_H. With this explanation, one could assume that the high-energy cutoff is the more fundamental quantity that leads to a particle's rest energy equal to the reduced cutoff energy, i.e. $mc^2 = \varepsilon_H/2\pi$. This interpretation has no problem with point-like particles, unlike the storage of the rest energy in the electric field surrounding a classical point charged particle. We have assumed ε_H operates as a sharp cutoff. This is likely unphysical, however, we apply the philosophy that if a simplistic approach appears to be adequate then we keep it until a more sophisticated one is needed.

The reaction mechanism by which Eq. (10) gives the rest energy of a very small black hole is presented as a Feynman-like diagram in Fig. 5. Within this framework the particle's rest energy is maintained by a stream of emissions each with a distribution of photon survival times. The average amount of energy contained in the stimulated emissions is mc^2 [see Eq. (10)] with an average time between emissions of $\hbar/2mc^2$. This timescale is reminiscent of the Zitterbewegung obtained via the Dirac equation [17]. A crude representation of a small black hole (particle) is depicted in Fig. 6. A "real" particle is more complex with a distribution of stimulated photon energies, each with their own randomly determined birth and survival times. Rare low-energy stimulated emission can probe regions much further away than $ƛ_C$. We here assume that the emission of each individual $L = 0$ stimulated-virtual photon, from an isolated particle, is in the form of a spherically symmetric outgoing wave that does not induce a recoil in the massless black hole. This will be modified in the next section to enable a description of the Lamb shift.

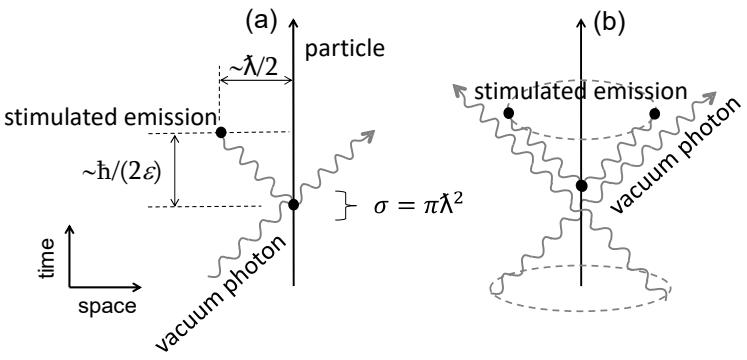

Fig. 5. Feynman-like diagrams of the proposed mechanism by which the rest energy of a very small black hole is stored in the surrounding cloud of stimulated-virtual photons generated by an interaction of the black hole with the vacuum-virtual photons. In each of the diagrams (a) and (b) there is only a single vacuum photon and a single stimulated emission. Diagram (a) depicts the direction reversing nature of the stimulated emission. Diagram (b) is an attempt to illustrate the $L = 0$ nature of both the initial interaction and the following stimulated emission with left and right going photons in the plane of the page. The dashed ellipses signify the isotropic nature of the $L = 0$ ingoing and outgoing vacuum photon and outgoing stimulated emission.

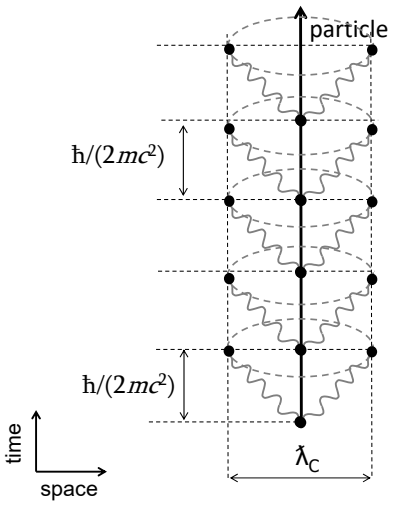

Fig. 6. A crude representation of a very small black hole (particle). Only the average stimulated-virtual-photon emission energy is depicted with these emissions travelling their average distance, with an average time of $\hbar/2mc^2$ between emissions. This gives an effective particle size of $\sim \lambda\!\!\!^{-}_C = \hbar/mc$. The stimulating vacuum-virtual photons are not shown. A real particle is more complex (see text).

The concept that the rest-mass energy of a particle is contained within a surrounding cloud of stimulated-virtual photons automatically gives the correct average relativistic energy and momentum (and thus inertia) as a function of the particle's velocity, via the Doppler shift of the stimulated-virtual photons associated with a particle's velocity. As a quick and simple demonstration of this effect, we consider Fig. 6 in an inertial reference frame where the particle is moving with a constant velocity v. In this reference frame, the average $\varepsilon = mc^2$ photon emissions parallel and anti-parallel to the direction of the velocity are Doppler shifted to energies of $\gamma(v)mc^2(1+v/c)$ and $\gamma(v)mc^2(1-v/c)$. The average of these energies gives the energy of a particle as $E = \gamma(v)mc^2$. Similarly, averaging the forward and backward photon momenta gives the particle momentum $p = \gamma(v)mv$. It is a simple exercise for the reader to see that these results are not changed by the integration over the continuous range of allowed photon energies and emission angles in the center-of-mass frame. An astute reader will know this is self-evident and requires no proof.

A semi-classical picture of why particles can "erupt" from the vacuum for a short time period is also obtained. This is because of the interpretation that the rest energy is stored in the surrounding cloud of stimulated-virtual photons, and not in the black hole (point-like particle) in the middle of the cloud. If a naked black hole (point-like particle) is born at time t=0 (without its cloud of stimulated-virtual photons) it will take a finite timescale for the first vacuum-virtual photon to find the new particle and start the generation of the surrounding virtual-photon cloud. This timescale is the inverse of the rate given by Eq. (9) and is equal to $\pi\hbar/\varepsilon_H = \hbar/2mc^2$, in agreement with the timescale that a particle anti-particle pair, with total mass m, can pop into existence before disappearing back into the vacuum as controlled by the time-energy uncertainty principle. This is not surprising, because the time-energy uncertainty principle is one of the inputted assumptions. What is of interest is that a simple semi-classical picture emerges, and that this picture is only self-consistent with the time-energy uncertainty principle if the high-energy cutoff is $\varepsilon_H = 2\pi mc^2$.

Another potentially pleasing possibility of the presented framework is that black holes cannot be smaller than the Planck length [18]. Macroscopic black holes with masses larger than the Planck mass have a Schwarzschild radius of $2m$ (in Planck units), while microscopic black holes with masses less than the Planck mass have an effective radius of $\sim \lambda\!\!\!^{-}_C/2$ (see Fig. 6) $\sim 1/2m$ (in Planck units). These macro- and microscopic radii suggest a black hole radius of $\sim 2m + 1/2m$ with a minimum radius of about two Planck lengths, at a mass of about one-half a Planck mass. In this picture macroscopic black holes store their rest energy inside the event horizon, while microscopic black holes store their rest energy in a surrounding cloud of virtual photons. This implies that a pair of macroscopic black holes will interact primarily via gravity, while a pair of microscopic black holes will interact primarily through their surrounding clouds of virtual photons.

Much of the rest of this manuscript is an attempt to support the idea that L=0 photon exchanges between a pair of chargeless small black holes (particles) can generate an electromagnetic force between them. This force can be used to estimate the numerical value of the fine-structure constant and thus the corresponding fundamental unit of charge, $e=(\alpha\hbar c4\pi\varepsilon_0)^{1/2}$. Before estimating the fine-structure constant it is important to first constrain other details that appear important to a semi-classical understanding of virtual-photon black hole (particle) interactions by modifying the above presented picture to obtain several electron-like properties.

V. Hydrogen Lamb shift

According to the Dirac equation, the hydrogen $2s_{1/2}$ and $2p_{1/2}$ levels are degenerate if a pure inverse-square-law Coulomb force is assumed to operate between the electron and the proton. There are several reasons why the true interaction is not a perfect inverse-square law at small distances. These include the finite size of the proton, vacuum polarization associated with virtual electron-positron pairs [19], and a possible intrinsic fuzziness of the electromagnetic interaction involving electrons on small length scales. In 1947 Lamb and Retherford [20] demonstrated that the hydrogen $2s_{1/2}$ level sits ~1000 MHz above the $2p_{1/2}$ level. Bethe showed in the same year [21] that this observation was predominantly due to the electromagnetic vacuum interacting with the electron, causing an intrinsic fuzziness in the electromagnetic interaction. A more modern measurement of the Lamb shift is 1057.85 MHz and is consistent with QED calculations [22].

From the Darwin term in the Dirac equation it follows that the hydrogen Lamb shift, to lowest order, is [17]

$$\Delta E_{2s} = \frac{2\pi}{3}\alpha\hbar c\ \delta r^2\ |\psi_{2s}(0)|^2 = \frac{2\pi}{3}\alpha\hbar c\ \delta r^2\ \frac{1}{4\pi}\frac{\alpha^3}{2\lambda\!\!\!^{-3}_{C}} = \frac{\alpha^4\hbar c}{12\lambda\!\!\!^{-3}_{C}}\ \delta r^2\ , \qquad (11)$$

where δr^2 is the root-mean-squared spread in the electron's location associated with its interaction with the electromagnetic vacuum. Eq. (11) can also be obtained via non-relativistic Schrödinger quantum mechanics using first-order perturbation theory.

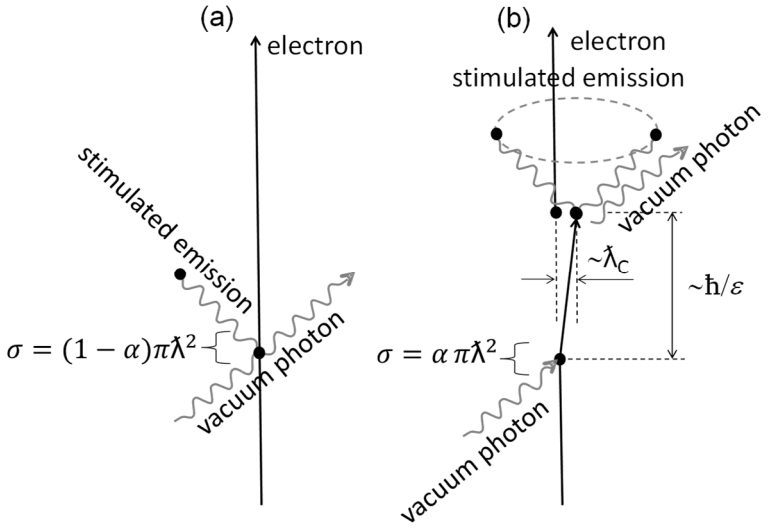

Fig. 7. Feynman-like diagrams for the reaction mechanism used to obtain Eq.s **(**12**)** and **(**13**)** (the Lamb shift). These diagrams are similar to Fig. 5 but divide the vacuum-photon particle interaction into a recoil-less interaction (a) and a recoiling interaction (b). In the recoiling interaction an isotropic stimulated-virtual photon is emitted at the end of the recoil before the electron's return to its original location. To keep the total interaction cross section of $\pi\lambda\!\!\!^{-2}$ and keep the particle's rest mass from changing from the result given in the previous section, the recoil-less reaction cross section is reduced to $(1-\alpha)\pi\lambda\!\!\!^{-2}$, to accommodate the recoiling interaction cross section of $\alpha\pi\lambda\!\!\!^{-2}$.

Here we modify the photon-electron interaction as discussed above (see Fig. 4 and Fig. 5) in a manner that does not change previously obtained results but leads to a simple description of the hydrogen Lamb shift. We make the ansatz that the interaction depicted in Fig. 4 and Fig. 5 is divided into recoil-less and recoiling interactions with cross sections of $(1-\alpha)\pi\lambda\!\!\!^{-2}$ and $\alpha\pi\lambda\!\!\!^{-2}$, respectively, with the fine-structure constant α being the recoiling fraction. This modification to the photon-electron interaction is summarized in Fig. 7 and leads to a fuzziness in an electron's location due to its interaction with the vacuum state. The recoil-less interaction is unchanged from Fig. 5, except for a small drop in its cross section [see Fig. 7(a)]. For the recoiling interaction, the incident vacuum-virtual photon of energy ε is assumed to, at first, be absorbed by the electron, violating energy conservation for a small time period of $\hbar/\varepsilon$, while maintaining conservation of momentum with a particle recoil velocity $v = \varepsilon/(mc)$. To re-establish conservation of energy after the short time period of $\hbar/\varepsilon$, we assume the absorbed vacuum-virtual photon is returned to the vacuum and the electron is returned to its original location as though the recoil interaction had not occurred [see Fig. 7(b)]. We are assuming the acts of vacuum-photon absorption and emission back into the vacuum each take a timescale of $\hbar/2\varepsilon$ to complete, i.e. a combined timescale of $\hbar/\varepsilon$. This gives an average recoil distance of $r = v\hbar/\varepsilon = \hbar/mc = \lambda\!\!\!^{-}_{C}$. This recoil distance is obtained here in the non-relativistic limit. However, the same result is obtained with relativistic kinematics if the timescale of $\hbar/\varepsilon$ is assumed to apply in the reference frame of the recoiling particle. The emission of the stimulated-virtual photon associated with the recoiling interaction is assumed to be isotropic and to occur at the end of the recoil, but before the electron's return to its pre-absorption state as depicted in Fig. 7(b). This assumption is not

required to give the Lamb shift but is introduced here because it leads to a reproduction of the known anomalous magnetic moment of the electron in the next section.

The electron blurring mechanism depicted in Fig. 7 naturally leads to higher-order corrections not considered here. For example, while in the act of recoiling, an electron can interact with another (independent) incident virtual-vacuum photon. These overlapping recoil events will be rare. In analogy to higher-order corrections associated with the magnetic moment of the electron, we assume the next higher-order interactions will modify results by an amount proportional to $\sim\alpha/\pi$ [23]. This is a recurring theme in this paper.

Given the probability per unit time to complete the combined absorption and re-emission process is assumed to be $\varepsilon/\hbar$ (as discussed above) then there will be an exponential ensemble of recoil distances with probabilities of $\exp(-r/\lambda\!\!\!^{-}_{\mathrm{C}})$, and a mean value of $\lambda\!\!\!^{-}_{\mathrm{C}}$. For a given recoil distance r, the rms spread of the electron's location averaged along its path is $r^2/3$ (assuming a constant recoil velocity), with a recoil time of rmc/ε. Combining these effects gives a rms spread in an electron's location due to the recoils associated with the absorption and re-emission of vacuum-virtual photons of

$$\delta r^2(\varepsilon)=\frac{\int_0^\infty \frac{r^2}{3}\frac{rmc}{\varepsilon}\frac{\alpha d\varepsilon}{\pi\hbar}\exp(-r/\lambda\!\!\!^{-}_{\mathrm{C}})dr}{\int_0^\infty \exp(-r/\lambda\!\!\!^{-}_{\mathrm{C}})dr}=\frac{\alpha mc^2}{3\lambda\!\!\!^{-}_{\mathrm{C}}\pi\hbar c}\frac{d\varepsilon}{\varepsilon}\int_0^\infty r^3\exp\left(-\frac{r}{\lambda\!\!\!^{-}_{\mathrm{C}}}\right)dr=\frac{2\alpha\lambda\!\!\!^{-2}_{\mathrm{C}}}{\pi}\frac{d\varepsilon}{\varepsilon}. \quad (12)$$

This is the same result obtained by Welton [24,17] using a wave-based picture of the electromagnetic vacuum, and partially justifies the presented particle-based description with an electron-recoil fraction α, and the total absorption and re-emission timescale of $\hbar/\varepsilon$ which causes a delay of the same time between the initial interaction and the eventual emission of the stimulated-virtual photon, as summarized in Fig. 7(b). Integrating Eq. (12) over the energy of the relevant vacuum-virtual photons gives the result

$$\delta r^2=\frac{2\alpha\lambda\!\!\!^{-2}_{\mathrm{C}}}{\pi}\int_{\varepsilon_{\mathrm{L}}}^{\varepsilon_{\mathrm{H}}}\frac{d\varepsilon}{\varepsilon}. \quad (13)$$

To obtain a finite result using Eq. (13) there need to be both low- and high-energy cutoffs. A possible value for the high-energy cutoff is discussed above ($\varepsilon_{\mathrm{H}}=2\pi mc^2$). The nature of the Lamb shift is such that the rms spread of the electron only significantly affects the energy of s-state electrons due to their non-negligible probability of being within $\sim\lambda\!\!\!^{-}_{\mathrm{C}}$ of the proton, where the absolute value of the electron's potential energy is $\sim\alpha mc^2$. This is the value of the traditional Lamb-shift low-energy cutoff, $\varepsilon_{\mathrm{L}}=\alpha mc^2$, used in other semi-classical descriptions of the Lamb shift [17]. We choose to use the same value here and obtain

$$\delta r^2\sim\frac{2\alpha\lambda\!\!\!^{-2}_{\mathrm{C}}}{\pi}\int_{\alpha}^{2\pi}\frac{d\varepsilon}{\varepsilon}\sim\frac{2\alpha\ln(2\pi/\alpha)\lambda\!\!\!^{-2}_{\mathrm{C}}}{\pi}\quad\text{and}\quad\Delta E_{2s}\sim\frac{\alpha^5\ln(2\pi/\alpha)}{6\pi}mc^2\sim 1000\ \text{MHz}. \quad (14)$$

To be clear, only plausibility arguments are used here (not proofs) and as with many semi-classical approaches it is up to the reader to decide if the level of agreement with experiment indicates some truth in the used assumptions or is simply wishful thinking by the author. However, the presented semi-classical description divides the physics of the Lamb shift into several relatively easy to understand steps including: (1) an $L=0$ interaction between vacuum-virtual photons and electrons, with a cross section of $\pi\lambda\!\!\!^{-2}$; (2) multiplied by the probability α, that this interaction induces an electron recoil; and (3) with a recoil timescale of $\hbar/\varepsilon$ associated with the time required to both absorb and then re-emit the vacuum-virtual photons. These assumptions are not the only semi-classical particle-based scheme capable of giving the Lamb shift. From an array of different schemes that give the same results, we chose to use the one that can be represented by the simplest Feynman-like diagram.

VI. Anomalous magnetic moment of the electron

As a heads up to the reader, this section is long, possibly tedious, and contains several unorthodox assumptions to enable the presented particle-based picture to match the known magnetic properties of the electron. The reason for the detailed analysis of magnetic moments in this section is not to show that the presented particle-based picture is in agreement with the magnetic properties of the electron, but that within this picture we can constrain the properties of stimulated-virtual-photon electron self-absorptions so we can apply these nearly unchanged to the calculation of photon exchanges between an electron pair in the next section. In this section, the length scale of near-field effects is adjusted to give the anomalous magnetic moment of free electrons, and a self-interaction high-energy cutoff is adjusted to give the correct dependence of the magnetic moment of electrons, in hydrogen-like atoms (and ions), on the atomic number of the nucleus.

To obtain a simple picture of the anomalous magnetic moment of the free electron, we are at first guided by the fact that in QED the anomalous magnetic moment is caused by the emission and reabsorption of virtual photons. Within the framework presented here, a similar-looking process can be obtained by assuming that the stimulated-virtual photon emission at the end of the Lamb-shift-related recoil can be self-absorbed by the same electron after its jump back to its original location (see Fig. 8). We assume the cross section for this self-absorption is $\pi\lambda\!\!\!^{-2}$ if the distance between the photon-birth and self-interaction locations d is very much larger than $\lambda\!\!\!^{-}$, but with a new high-energy self-interaction cutoff, $\mathcal{E}_S < \mathcal{E}_H$, that is influenced by the state of the electron, and more specifically by how it is interacting with any nearby particles. The corresponding self-absorption probability is $P_S = \pi\lambda\!\!\!^{-2}/4\pi d^2$ for photons with energies $< \mathcal{E}_S$. We assume the self-absorption high-energy cutoff $\mathcal{E}_S$ is inversely proportional to the size of the system within which the electron is operating. Therefore, free and/or quasi-free electrons in a macroscopic trap have a very small self-absorption high-energy cutoff. Inspired by Bekenstein and Meirels' work on black holes we assume the self-absorption of a stimulated-virtual photon stimulates the generation of a stimulated-virtual photon that retraces the path of the incident stimulating photon (see Fig. 8).

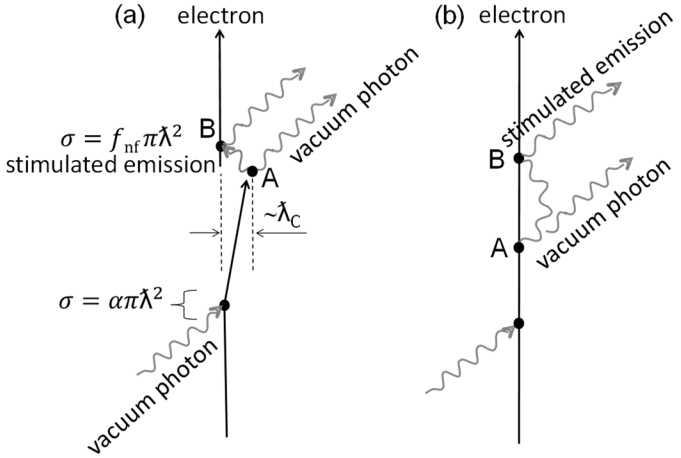

Fig. 8. Feynman-like diagram for the reaction mechanism used here to obtain a simple representation of the anomalous magnetic moment of a free electron. (a) Almost the same diagram as shown in Fig. 7(b). The only difference is that the stimulated-virtual photon emitted at the end of the electron recoil (from point A) "finds" the electron soon after its "return" to its pre-recoil location (at point B) and is self-absorbed. This absorption generates a direction-reversed stimulated emission. Straightening out the electron's path gives the diagram to the right (b). Removing the ingoing and outgoing virtual photons gives the standard Feynman diagram for the anomalous magnetic moment.

Given the exponential distribution of Lamb-shift related recoil distances (see the previous section), the probability that a stimulated-virtual photon emitted at the end of the recoil is self-absorbed at point B (see Fig. 8), can be expressed as

$$P_S = \frac{\int_0^\infty \int_0^{\varepsilon_S} \frac{\pi \lambda\!\!\!^{-2}}{4\pi x^2} \exp\left(\frac{-x}{\lambda\!\!\!^{-}_C}\right) dx\, d\varepsilon}{\int_0^\infty \int_0^{\varepsilon_S} \exp(-x/\lambda\!\!\!^{-}_C) dx\, d\varepsilon} = \frac{1}{\lambda\!\!\!^{-}_C \varepsilon_S} \int_0^\infty \int_0^{\varepsilon_S} \frac{\hbar^2 c^2}{4x^2\varepsilon^2} \exp\left(\frac{-x}{\lambda\!\!\!^{-}_C}\right) dx\, d\varepsilon. \quad (15)$$

This can be further simplified by switching to energy and length in units of mc^2 and $\lambda\!\!\!^{-}_C$, giving

$$P_S = \int_0^\infty \int_0^{\varepsilon_S} \frac{1}{4x^2\varepsilon^2} \exp(-x) \frac{dx\, d\varepsilon}{\varepsilon_S}. \quad (16)$$

This equation gives the unphysical result of an infinite probability due to the $1/x^2$ and $1/\varepsilon^2$ terms. This situation can be rectified by the realization that near-field effects will introduce an effective low-energy cutoff by modifying the absorption cross section for photons "falling" towards an electron from a finite starting distance d.

In the case of the communication between classical dipole antennas, the power exchange can be obtained using the far-field approximation when the antenna separation distance is more than a few times the physical dimension of the antennas. However, near-field effects start growing rapidly as the antenna separation decreases through twice their physical size. Experiments indicate the near-field effect for a pair of classical dipole antennas is of the form [25]

$$P(d,\delta) \sim \left(1 - \exp(\frac{-d}{\delta})\right) \cdot P(d), \quad (17)$$

where $P(d,\delta)$ is the power exchange between two antennas separated by a distance d; $P(d)$ is the far-field power exchange; $f_{nf}=(1-\exp(-d/\delta))$ is the near-field correction with the length scale δ a little larger than the size of the antennas [25]. For the self-absorption of $L=0$ stimulated-virtual photons, the far-field self-absorption cross section of $\pi\lambda\!\!\!^{-2}$ for $d >> \lambda\!\!\!^{-}$ and $\varepsilon < \varepsilon_S$, is consistent with an effective semi-classical antenna size of $\sim\lambda\!\!\!^{-}$. In analogy with classical dipole antennas we suspect the $L = 0$ self-absorption cross section to be of the form $f_{nf}\pi\lambda\!\!\!^{-2}$, with the near-field correction factor making a transition from unity at distances more than a few $\lambda\!\!\!^{-}$, to zero at length scales much less than $\lambda\!\!\!^{-}$. But what are the details of this transition?

With $d >> \lambda\!\!\!^{-}$ an electron pair must act as two independent interaction sites. When d is much less than $\lambda\!\!\!^{-}$ the electron pair will behave as a collective unit. Near-field effects, in the case of an electron pair, are depicted in Fig. 9. An incident vacuum photon interacts with an electron pair as a collective unit, in Fig. 9(a), generating a stimulated-virtual photon that exits from the pair. In this case the stimulated photon is not available for an exchange between the individual electrons as the interaction only sees the pair as a collective unit. An incident vacuum photon interacts with the electrons as independent units, in Fig. 9(b), generating stimulated-virtual photons that are emitted from the individual electrons. In this case the stimulated photon is available for an exchange between the individual electrons in the pair. The near-field factor, f_{nf}, reduces the interaction cross section for an incident vacuum-virtual photon to interact with a given electron (as a single unit) due to the presence of a nearby partner. Similarly, the cross section for the corresponding stimulated emission to interact with the partner electron is also reduced by the same factor f_{nf}. The total interaction cross section between a vacuum-virtual photon and an electron pair is the collective interaction cross section [see Fig. 9(a)], plus twice the individual interaction cross section [see Fig. 9(b)], and must be $2\pi\lambda\!\!\!^{-2}$. This is necessary to keep the proposed electromagnetic interaction, in the next section, a simple two-body force.

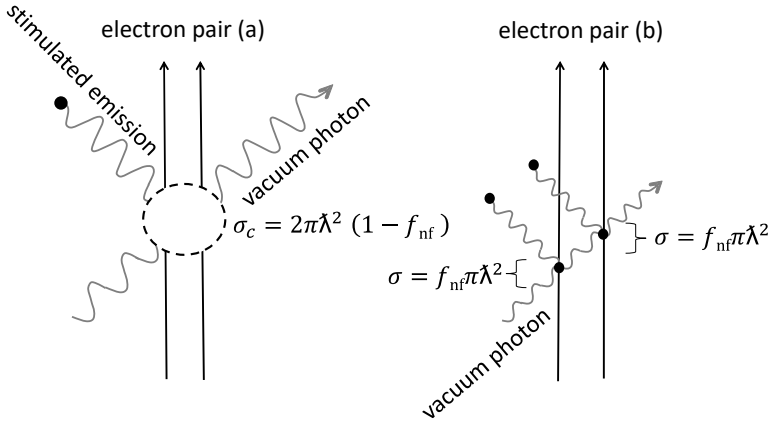

Fig. 9. A depiction of near-field effects associated with an electron pair. (a) A vacuum-virtual photon with a reduced wavelength larger than the pair's separation distance interacts with the pair as a collective unit generating a stimulated-virtual photon that exits from the pair. (b) A vacuum-virtual photon with a reduced wavelength smaller than the pair's separation distance interacts with the electrons as individual units generating stimulated-virtual photons that can be exchanged with the other particle.

We make the ansatz that the transition from independent electrons to collective behavior is governed by the overlap of harmonic-oscillator ground-state wave functions (Guassians)

$$\psi(r) \propto \exp\left(\frac{-r^2}{2a^2\lambda\!\!\!^{-2}}\right), \tag{18}$$

with the photon-electron interaction probability per unit volume proportional to ψ^2. The constant "a" scales the spatial extent of the interaction wave function relative to $\lambda\!\!\!^{-}$, and will soon be determined by the magnetic moment of the electron (to second order) in conjunction with some other assumptions. We further assume that the cross section for either of the electrons, in a pair, to interact with a photon as a single unit is given by

$$f_{\rm nf} \cdot \pi\lambda\!\!\!^{-2} \propto \int \left[\psi(\tilde{r}) - \psi(\tilde{r} - \tilde{d})\right]^2 dr^3 = \pi\lambda\!\!\!^{-2}\left\{1 - \exp\left(-\left(\frac{d}{2a\lambda\!\!\!^{-}}\right)^2\right)\right\}. \tag{19}$$

The corresponding cross section for a single photon to interact with both electrons as a collective pair then has to be

$$\sigma_{\rm c} = 2\pi\lambda\!\!\!^{-2}\exp\left(-\left(\frac{d}{2a\lambda\!\!\!^{-}}\right)^2\right), \tag{20}$$

as required by the above discussion of the total interaction cross section. Notice that for $d << \lambda\!\!\!^{-}$ an electron pair behaves as a collective unit; for $d >> \lambda\!\!\!^{-}$ the electrons in a pair behave as separate (individual) units; and the constant "a" controls the length scale for the transition between these two limiting cases. Including the near-field effects as expressed in Eq. (19) into Eq. (16) leads to the finite result

$$P_{\rm S} = \int_0^{\infty}\int_0^{\varepsilon_{\rm S}}\left\{1 - \exp\left(-\left(\frac{x\varepsilon}{2a}\right)^2\right)\right\}\exp(-x)\,\frac{dx\,d\varepsilon}{4x^2\varepsilon^2\varepsilon_{\rm S}}. \tag{21}$$

We have assumed, in the case of an isolated electron, that the initial interaction towards the bottom of Fig. 8(a) has the far-field cross section of $\pi\lambda\!\!\!^{-2}$ multiplied by the recoil fraction α, while the self-absorption cross section at point B needs to be near-field corrected due to the closeness of point A. For a very low-energy electron (in a large macroscopic trap), we set the cutoff energy $\varepsilon_{\rm S}$ to be very small, and rewrite Eq. (21)

$$P_S = \int_0^\infty \int_0^{\varepsilon_S} \frac{x^2\varepsilon^2}{4a^2} \exp(-x) \frac{dx\, d\varepsilon}{4x^2\varepsilon^2\varepsilon_S} = \frac{1}{(4a)^2}. \quad (22)$$

The cancelation of length-scale and energy terms makes the self-absorption probability very insensitive to the properties of low-energy electrons. This is a requirement for the existing model to be consistent with experiment. We make the additional ansatz that the self-absorption of a stimulated-virtual photon by an isolated electron and the subsequent direction-reversed stimulated emission, at point B in Fig. 8, enables the generation of a magnetic moment of one Bohr magneton, μ_B, in the direction of the electron's spin for a time period $\tau_m = \pi\hbar/\varepsilon_S$; and this magnetism is in addition to the standard intrinsic magnetic moment associated with the Dirac equation. We have no strong arguments for these assumptions other than invoking them gives the desired result presented below. However, as weak plausibility arguments, the choice of a particle magnetic moment of one Bohr magneton feels natural because a charged particle with a single unit of orbital angular momentum generates one Bohr magneton; and the self-absorption magnetic generation time of $\tau_m = \pi\hbar/\varepsilon_S$ may be related to the Zitterbewegung timescale of $\hbar/2mc^2 = \pi\hbar/\varepsilon_H$ but with the high-energy cutoff ε_H replaced by the self-absorption high-energy cutoff, ε_S.

As discussed above, the rate of stimulated-virtual-photon emission following a Lamb-shift related recoil is $\alpha\varepsilon_H/(\pi\hbar)$. Only $\varepsilon_S/\varepsilon_H$ of these emissions are available for a self-absorption with $1/(4a)^2$ of these self-absorption attempts being successful. Including the magnetic-moment generation time introduced above, the average anomalous magnetic moment of the free electron is

$$\frac{g-2}{2} = \frac{\alpha\varepsilon_H}{\pi\hbar} \frac{\varepsilon_S}{\varepsilon_H} \frac{1}{(4a)^2} \cdot 1 \cdot \frac{\pi\hbar}{\varepsilon_S} = \frac{\alpha}{(4a)^2}. \quad (23)$$

This can be made to agree with second-order QED by setting $a = (\pi/8)^{1/2} = 0.626657\ldots$. This corresponds to a self-absorption probability of $P_S = 1/2\pi$.

It may appear as if unjustified assumptions have been made to generate the correct answer. However, the proposed reaction mechanisms can be tested by the calculation of their additional consequences as done below. Before moving on to a calculation of the fine-structure constant we constrain the self-absorption high-energy cutoff, ε_S. We do this in the next subsection via a study of the change in the magnetic moment associated with electrons in hydrogen-like atoms (ions) as a function of the charge and mass of the atomic nucleus.

VI.A Magnetic moment of the electron in hydrogen-like systems

The interplay between the far-field interaction cross section and near-field effects gives the result that, even in the limit as the size of the electron recoil goes to zero, $1/2\pi$ of the stimulated emissions with $\varepsilon \leq \varepsilon_S$ are self-absorbed by an isolated electron [See Eq. (22) with $a = (\pi/8)^{1/2}$]. This leads to the interesting possibility that $1/2\pi$ of the stimulated emissions following recoil-less interactions with $\varepsilon \leq \varepsilon_S$ are also self-absorbed by an isolated electron, followed by a direction-reversed stimulated emission. If true, then there are four ways by which a vacuum-virtual photon, with $\varepsilon \leq \varepsilon_S$, can interact with an isolated electron (see Fig. 10). The total rate of self-absorptions would then be $\varepsilon_S/\pi\hbar$ divided by 2π with a fraction α following recoils associated with the Lamb shift, and a fraction $1-\alpha$ following recoil-less interactions with vacuum photons (see Fig. 10). If the stimulated-virtual photon self-absorptions that follow the Lamb-shift-related recoils generate magnetism then so might all self-absorptions, including those following recoil-less interactions. However, all of the magnetic moment of the electron has been accounted for with the intrinsic value from the Dirac equation plus the anomalous value from the previous subsection. We "solve" this problem by making the ansatz that any magnetic moment generated by the self-absorptions following recoil-less vacuum-photon interactions is a part of the intrinsic magnetic moment associated with the

Dirac equation. This assumption is unorthodox and gives a breakdown of the magnetic moment of the free electron as displayed in Fig. 11.

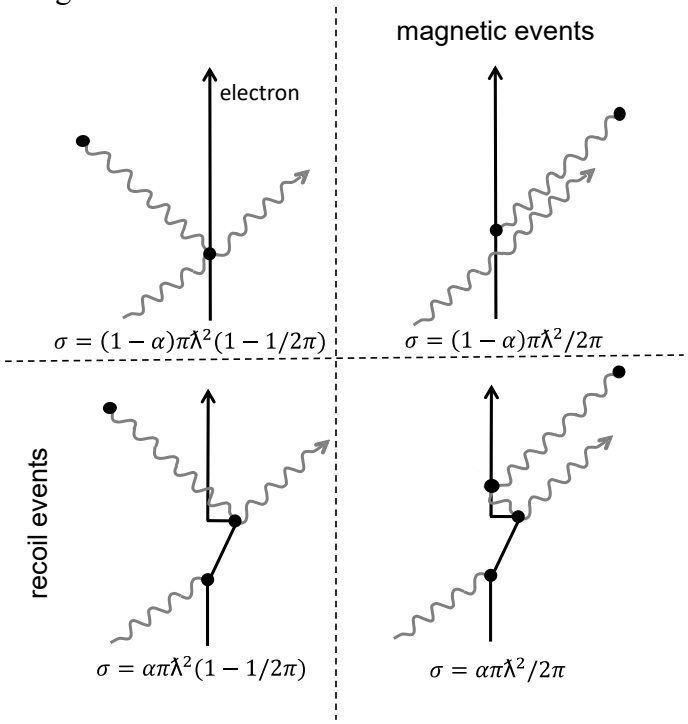

Fig. 10. A summary of the four different ways in which a vacuum-virtual photon, with $\varepsilon < \varepsilon_S$ can interact with an electron with the corresponding event cross sections, σ. Notice that the total interaction cross is still $\pi\lambda\!\!\!^{-2}$. The event classes on the right induce magnetism (see text). The event classes on the bottom involve an electron recoil.

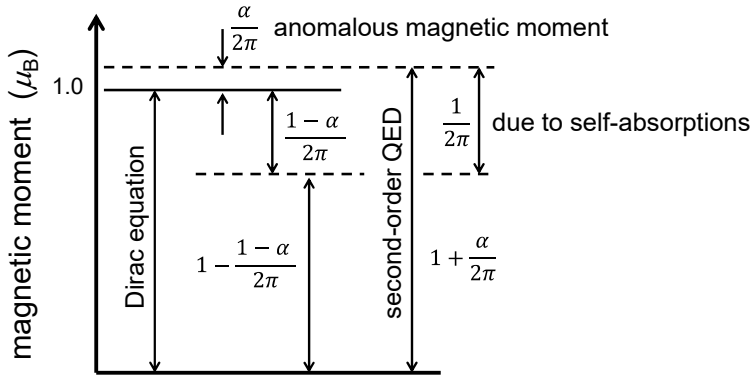

Fig. 11. Different components of the magnetic moment of the free electron.

Within this framework, $\mu_B/2\pi$ of the magnetic moment is due to self-absorptions of stimulated-virtual photons (see Fig. 11). This component can be divided into two parts. For free electrons, these are $\alpha\mu_B/2\pi$ and $(1-\alpha)\mu_B/2\pi$. The $\alpha\mu_B/2\pi$ component is associated with the self-absorptions following the displacement of the electron that causes the Lamb shift, and is the anomalous magnetic moment in excess of the intrinsic magnetic moment associated with the Dirac equation. The $(1-\alpha)\mu_B/2\pi$ component is also initiated by self-absorptions, but associated with interactions with no consequence on the Lamb shift, and assumed to be a part of the intrinsic magnetic moment of the free electron as obtained by the Dirac equation. The $\alpha\mu_B/2\pi$ component varies with the size of the electron trap via the self-absorption high-energy cutoff, ε_S. This dependency on the state of the electron can be determined via Eq. (21). It is

reasonable to assume that the $(1-\alpha)\mu_B/2\pi$ component has the same dependence on the size of the electron trap.

The self-absorption probability of $P_S = 1/2\pi$ from Eq. (22) with $a = (\pi/8)^{1/2}$ is obtained via the assumption that the electron is free or, at least, in a large macroscopic trap. Hydrogen-like atoms (ions) can be viewed as microscopic traps. Based on the discussion in the previous subsection, the size of the self-absorption high-energy cutoff will increase with a decrease in the size of an electron's orbital, and thus increase with the atomic number of the nucleus of a hydrogen-like atom. A representation of the electron's magnetic moment as a function of the atomic number of the nucleus in a hydrogen-like atom can be obtained by assuming the high-energy cutoff for the stimulated-virtual-photon self-absorption cross section is given by the energy of a photon whose wavelength is the return distance from the electron to the associated partner particle and back; i.e. $\varepsilon_S = hc/2d = \pi\hbar c/d$. This value can be partially justified because the magnetic generation time introduced in the previous subsection and the Zitterbewegung timescale are both given by $\pi\hbar$ divided by the corresponding energy cutoff, and thus energy cutoffs appear to be $\pi\hbar$ divided by a relevant timescale. For a two particle system it seems reasonable that the relevant timescale would be d/c. For electron-nucleus ground-state systems, we replace d with the corresponding Bohr radius, giving $\varepsilon_S = \alpha\pi Zmc^2$. Incorporating this into Eq. (21) gives

$$P_S = \int_{x=0}^{\infty}\int_{\varepsilon=0}^{\alpha\pi Z}\left(\frac{2x^2\varepsilon^2}{\pi} - \frac{2x^4\varepsilon^4}{\pi^2} + \cdots\right)\exp(-x)\frac{dx\,d\varepsilon}{4x^2\varepsilon^2\alpha\pi Z} = \frac{1}{2\pi} - \frac{\alpha^2Z^2}{3}. \quad (24)$$

Including the other assumptions discussed above, and the fact that a finite nuclear mass, M, modifies the distance between the electron and the nucleus by a factor of $1+m/M$, Eq. (24) translates into a Z dependence of the magnetic moment of the electron in hydrogen-like atomic ground states relative to the Bohr magneton of

$$\begin{aligned}\frac{\mu_e(1s)}{\mu_B} &= 1 - \frac{1-\alpha}{2\pi} + \frac{1}{2\pi} - \frac{\alpha^2Z^2}{3}\left(1 - \frac{2m}{M}\right)\\ &= 1 + \frac{\alpha}{2\pi} - \frac{\alpha^2Z^2}{3}\left(1 - \frac{2m}{M}\right). \end{aligned} \quad (25)$$

in agreement with standard theory to the same order in α and m [26]. Higher-order effects [27] and subtleties associated with details in the shape of the electron wave function [28] modify Eq. (25) and give

$$\frac{\mu_e(1s)}{\mu_B} = 1 + \frac{\alpha}{2\pi} - \frac{\alpha^2Z^2}{3}\left(1 - \frac{3m}{2M}\right) + \frac{\alpha^3Z^2}{12\pi}\ . \quad (26)$$

Of course, even higher-order corrections exist [29]. Measured magnetic moments of free and bound electrons are compared to theory and the model presented here in Table I. The results listed in Table I partially justify the assumptions used in this section. However, the reader should remember that the used assumptions were not derived by first principles, but adjusted to reproduce known experimental results. These assumptions include: (a) photon-electron interaction near-field corrections are governed by the overlap of ground-state harmonic-oscillator wave functions with the spatial extent of these wave functions adjusted to give the known anomalous magnetic moment of the free electron; (b) self-absorptions generate one Bohr magneton for a timescale of $\tau_m = \pi\hbar/\varepsilon_S$; (c) for free electrons we take the limit as ε_S goes to zero, while for two-particle ground-state systems we set $\varepsilon_S = \pi\hbar c/d$ and set the separation distance d to the corresponding reduced-mass corrected Bohr radius; and (d) a constant intrinsic (system size independent) magnetic moment of $[1-(1-\alpha)/2\pi]\mu_B$, not associated with self-absorptions, was adjusted to give results in agreement with second-order QED (see Fig. 11).

Table I. A comparison of measured and calculated magnetic moments of free and bound electrons.

Magnetic moments	Experiment	Theory [29]	Eq. (25)
free electron (μ_B)	$1+1159.52181\times10^{-6}$ [4]	$1+\alpha/2\pi$	$1+\alpha/2\pi$
H/free	$1-17.709(13)\times10^{-6}$ [27]	$1-17.694\times10^{-6}$	$1-17.711\times10^{-6}$ *
D/H	$1-7.22(3)\times10^{-9}$ [30]	$1-7.24\times10^{-9}$	$1-9.61\times10^{-9}$ **
T/H	$1-10.7(15)\times10^{-9}$ [31]	$1-9.7\times10^{-9}$	$1-12.8\times10^{-9}$ **
$^4He^+$/free	$1-70.87(30)\times10^{-6}$ [32]	$1-70.91\times10^{-6}$	$1-70.90\times10^{-6}$ *
$^{12}C^{5+}$(μ_B)	$1+520.798(2)\times10^{-6}$ [33]	$1+520.795(1)\times10^{-6}$	$1+520.39\times10^{-6}$ ***

* Eq. (25) only includes effects to second-order (see Fig. 8) and thus these ratios are obtained using a free value of $1+\alpha/2\pi$.

** As discussed in the text, Eq. (25) only includes the size of the bound-electron orbitals. Subtleties in the details of the shape of the electron's wave function modify the nuclear mass correction coefficients by a factor of ¾ [28]. Including this factor gives agreement with experiment.

*** For the reason given in *, to better compare this value directly to the experimental value we have multiplied Eq. (25) by the ratio of the electron's free magnetic moment of 1.00115952181 μ_B to the corresponding value from second-order QED.

VII. Exchange of virtual photons between an electron pair

Given that electrons are indistinguishable, the self-absorption process from the previous section (as illustrated in Fig. 8) enables the stimulated-virtual photon emission from one electron to interact with a nearby separate partner electron as depicted in Fig. 12.

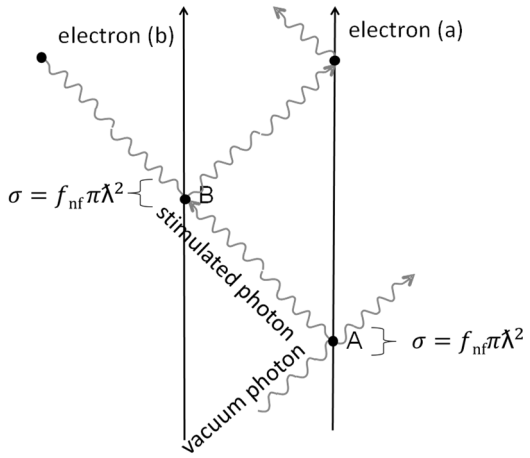

Fig. 12. Feynman-like diagram depicting the exchange of a stimulated-virtual photon between an electron pair. This is similar to Fig. 8, except here the stimulated-virtual photon emitted from point A interacts with a separate partner electron instead of with itself. As in the case of the self-absorption, the interaction at point B is assumed to stimulate a direction-reversed photon that starts at point B and travels back towards the partner electron. If this photon reaches the partner particle then an additional direction-reversed stimulated emission occurs which sends a photon back towards the other particle. This photon rattling is assumed to continue until one of the exchanging stimulated-virtual photons "disappears" via the time-energy uncertainty principle. Additional complexities are discussed in the text.

The rate of stimulated-virtual photon emission (with $\varepsilon < \varepsilon_S$) from point A (in Fig. 12), if electron (a) is isolated, is as given previously, $d\varepsilon/\pi\hbar$ (see Fig. 5). The presence of the partner electron (b) at a finite distance d, reduces the emission rate of stimulated-virtual photons that are capable of making an exchange to point B, by the near-field reduction factor, f_{nf}, as discussed in the previous section and depicted in Fig. 9. The probability that a stimulated-virtual photon emission from point A (in Fig. 12) interacts at point B is given by

$$\mathrm{p} = \frac{f_{\mathrm{nf}}\pi\lambda\!\!\!^{-2}}{4\pi d^2}\exp\left(\frac{-2\varepsilon}{\hbar}\frac{d}{c}\right) = \frac{f_{\mathrm{nf}}\pi\lambda\!\!\!^{-2}}{4\pi d^2}\exp(-\varepsilon/T_{\mathrm{ex}}), \tag{27}$$

with an effective exchange temperature $T_{\mathrm{ex}} = \hbar c/2d$. As in the case of the self-absorptions introduced in the previous section [see Eq. (21)], the f_{nf} term reduces the interaction cross section of the first stimulated-virtual photon with the partner electron at location B, due to the proximity of the partner particle. The exponential factor in Eq. (27) takes into account the probability that the stimulated-virtual photon "disappears" during the attempted exchange across the distance d. This term was not included in the previous section on self-absorptions because, in that case, the corresponding distances were small, of the order of $\lambda\!\!\!^{-}_{\mathrm{C}}$. This sets the corresponding $\exp(-\varepsilon/T_{\mathrm{ex}})$ terms to essentially unity in the self-absorption case. Given Eq. (27) one might, at first, think that the rate of stimulated-virtual photon exchange from point A to point B (see Fig. 12) is

$$\mathrm{R}_1(\varepsilon)d\varepsilon = \frac{f_{\mathrm{nf}}d\varepsilon}{\pi\hbar}\,\frac{f_{\mathrm{nf}}\pi\lambda\!\!\!^{-2}}{4\pi d^2}\exp(-\varepsilon/T_{\mathrm{ex}}) = \frac{f_{\mathrm{nf}}^2\,\hbar c^2}{4\pi d^2\varepsilon^2}\,\exp(-\varepsilon/T_{\mathrm{ex}})\,d\varepsilon\,. \tag{28}$$

However, we assume (at first) that the stimulated-virtual photon direction reversal following an exchange is "perfect" and thus the stimulated-virtual photon generated by electron (b), by an incident photon from electron (a), will automatically be heading in a direction to re-find particle (a), at least in the limit of low particle acceleration, as depicted in Fig. 12. With this picture the stimulated-virtual photon exchange rate from electron (a) to electron (b), due to vacuum-virtual-photon interactions that occurred a time $t = d/c$ earlier than point A (see left hand side of Fig. 13) is given by

$$\mathrm{R}_2(\varepsilon)d\varepsilon = \frac{f_{\mathrm{nf}}^2\,\hbar c^2}{4\pi d^2\varepsilon^2}\,\exp^2(-\varepsilon/T_{\mathrm{ex}})d\varepsilon. \tag{29}$$

Similarly, the exchange rate of stimulated-virtual photons from electron (a) to electron (b), due to vacuum-virtual-photon interactions that occurred a time $t = 2d/c$ earlier than point A (see right hand side of Fig. 13) is given by

$$\mathrm{R}_3(\varepsilon)d\varepsilon = \frac{f_{\mathrm{nf}}^2\,\hbar c^2}{4\pi d^2\varepsilon^2}\,\exp^3(-\varepsilon/T_{\mathrm{ex}})d\varepsilon. \tag{30}$$

The continuation of this exchange sequence gives the total stimulated-virtual-photon exchange rate from an electron to a partner electron as

$$\mathrm{R}(\varepsilon)d\varepsilon = \frac{f_{\mathrm{nf}}^2\,\hbar c^2}{4\pi d^2\varepsilon^2}\;\;\frac{d\varepsilon}{\exp(\varepsilon/T_{\mathrm{ex}})-1}. \tag{31}$$

Notice the introduction of the Planckian factor.

The continuation of the initiating photon at point A on the left hand side of Fig. 13 following the first exchange enables the original stimulated-photon emission from electron (b) to attempt to find a possible third electron. This is necessary for the electromagnetic interaction proposed here to give a simple two-body force. The interaction of an exchanging stimulated-virtual photon with an electron is depicted in Fig. 14. The probability for the exchanging photon to continue on after its interaction is $P = 1-\exp(-\varepsilon/T_{\mathrm{ex}}) = 1-\exp(-2d/\lambda\!\!\!^{-})$. This is not an assumption, but a requirement to cause there to be one continued exchanged photon (on average) per initial exchange initiated by a vacuum-virtual photon. This enables the number of stimulated photons that exit a pair of electrons, in search of a possible third particle, to be independent of the spacing between the electron pair. This is needed to keep the proposed electromagnetic interaction a simple two-body force. Notice the similarity of the exchanging photon's interaction (in Fig. 14) to the virtual-vacuum photon's interaction with a particle in Fig. 5. In the limit as $d\to\infty$ these two interaction classes became identical. Also, notice that in the limit as $d\to 0$, the probability that the initiating stimulated photon continues on its way becomes zero. This is consistent with Fig. 8 where there is no continuation of the stimulating-virtual photon towards the top left because, in this case, the distance d is very small.

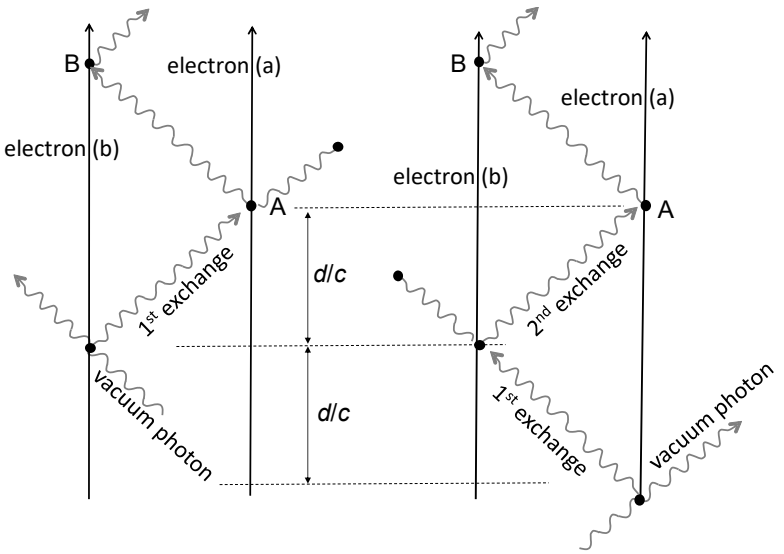

Fig. 13. Two Feynman-like diagrams depicting the exchange of stimulated-virtual photons between an electron pair. These diagrams are essentially the same as Fig. 12, but in the left diagram the initial stimulated-virtual photon is generated by a vacuum-virtual-photon interaction with electron (b) at time d/c before the time of the emission from point A. In the right diagram the initial stimulated-virtual photon is generated by a vacuum-virtual-photon interaction with an electron (a) at time $2d/c$ before the time of the emission from point A.

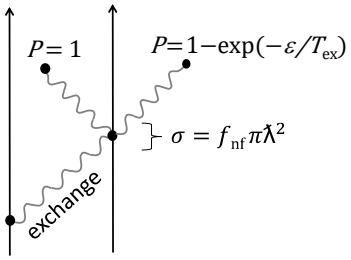

Fig. 14. The interaction of an exchanging stimulated-virtual photon with an electron. Here the stimulated direction-reversed photon is assumed to be generated with unity probability. The probability, $P=1-\exp(-\varepsilon/T_{ex})$, that the exchanging photon continues is a requirement needed to keep the proposed electromagnetic interaction a simple two-body force (see text).

We are now in a position to calculate the repulsive force between two electrons. In the earlier section on the rest mass of an isolated electron, where spherical symmetry was invoked, the emission of stimulated-virtual photons was assumed to impart no momentum to the emitting particle except in the case of rare short-lived recoils associated with the Lamb shift. However, in the case of an exchange between an electron pair, we assume the partner electron breaks spherical symmetry and that a photon exchange imparts a momentum of ε/c to each particle in the pair, away from its corresponding partner but, in a semi-classical sense, only after the exchange has been successfully completed. The momentum change to either particle per unit time associated with the second-order exchange of stimulated-virtual photons between them (see Fig. 12 and Fig. 13) is then given by

$$F \sim 2\int_0^{\varepsilon_S} \frac{f_{nf}^2\,\hbar c^2}{4\pi d^2\varepsilon^2}\,\frac{d\varepsilon}{\exp(\varepsilon/T_{ex})-1}\,\frac{\varepsilon}{c} = \frac{\hbar c}{2\pi d^2}\int_0^{\varepsilon_S}\frac{[1-\exp(-\varepsilon^2/2\pi T_{ex}^2)]^2}{[\exp(\varepsilon/T_{ex})-1]}\frac{d\varepsilon}{\varepsilon} \sim \frac{\alpha\hbar c}{d^2}. \qquad (32)$$

The high-energy cutoff, $\varepsilon_S = \pi\hbar c/d$, is the same value associated with the self-absorptions from the previous section. The factor of two on the left is because of the two possible directions for an exchange, i.e. from electron (a) to electron (b), and from (b) to (a). The integral in Eq. (32) is reminiscent of that used to obtain the Lamb shift in section V but with some additional factors. Switching Eq. (32) into energy in units of $T_{ex} = \hbar c/2d$ gives a compact result for the fine-structure constant to second order

$$\alpha \sim \frac{1}{2\pi}\int_0^{2\pi}\frac{[1-\exp(-\varepsilon^2/2\pi)]^2}{[\exp(\varepsilon)-1]}\frac{d\varepsilon}{\varepsilon} \sim \frac{1}{137.18\pm 0.32}\ , \tag{33}$$

with a corresponding fundamental unit of charge of (1.601±0.002)×10^{-19} C. The rough uncertainty estimate is in analogy with the analogous magnetic moment of the electron where the next order in QED adds a term of the order of α/π [23] smaller than the previous order.

It is important to realize that the above estimate of the fine-structure constant was obtained with adjustments that were made to obtain other QED observables. The form of the near-field corrections is based on an ansatz, but the corresponding 2π term was constrained by the anomalous magnetic moment of the electron along with other assumptions related to the generation of this magnetism. The 2π upper limit in the integration in Eq. (33) was constrained by the dependence of the magnetic moment of electrons in hydrogen-like atoms (and ions) on the atomic number of the nucleus. The $1/2\pi$ scaling, out the front, is due to the two way exchange divided by the 4π steradians available to isotopic emission. The exp(ε) term is associated with the time-energy uncertainty principle. There is only one adjustment not previously constrained by other QED processes (as outlined in the previous sections), i.e. the nature of the direction-reversing photon emission. Although introduced in the section on the anomalous magnetic moment of the electron and inspired by the calculated properties of black holes [15], the details of the corresponding photon rattle were not constrained by the anomalous magnetic moment. However, we claim that allowing the possibility of an infinite number of direction-reversing stimulated emissions, as in Eq.s (31) to (33), seems natural and leads to the pleasing Planckian factor. This Planckian factor is a general theoretical expectation for the quantum emission of photons [16]. It would be somewhat troubling if it was not present. The reader should be aware that allowing for an infinite number of direction-reversing stimulated emissions and the corresponding Planckian factor is what gives our semi-classical second-order estimate of α that is within a factor of ~α/π from the known value of ~1/137.036. Given the difference between Eq. (33) and 1/137.036 is less than α/π, it is possible that the difference might be removed by the inclusion of higher-order effects (see next subsection).

The force associated with the semi-classical exchange of stimulated-virtual photons between two particles, introduced here, can only generate repulsion. However, an attractive force between oppositely charged particles can be obtained by assuming the opposite charge is associated with a hole in a Fermi-sea of negative-energy particles [17, chap. 5].

VII.A Possible higher-order corrections to our α estimate

We do not have a detailed theoretical frame for the higher-order corrections that we seek. However, the form of Eq. (33) along with the various assumptions used to obtain it, suggest three likely ways in which it could be modified to include higher-order effects. These include modifications to: (a) the scaling of Eq. (33); (b) the 2π upper limit in the integration; and (c) the "−1" term in the Planckian factor due to the assumption that the direction-reversed photon emission following an exchange occurs with unit probability. This subsection does not prove that the suggested higher-order effects are real, but is more of a discussion on the possible nature of higher-order corrections that need to be explored further.

It is well known that second-order and higher-order QED effects increase the size of an isolated electron's magnetism from the Dirac equation result of one Bohr magneton, μ_B, by the factor [23]

$$\frac{g}{2} = 1 + \frac{\alpha}{2\pi} - 0.328478965\ldots\left(\frac{\alpha}{\pi}\right)^2 + 1.1812\ldots\left(\frac{\alpha}{\pi}\right)^3 + \cdots\ , \tag{34}$$

where g is the electron's gyromagnetic ratio that connects spin and magnetism. This relationship (including even higher-order corrections) is used to convert measurements of $g/2$ [or $(g-2)/2$] into our

most accurate inference of the fine-structure constant, $\alpha = 1/137.035999206(11)$ [5]. Here we assume that higher-order effects similar to those that increase the electron's magnetic moment relative to its corresponding zeroth-order value also increase the overall scaling of Eq. (33) by $1+\alpha/2\pi\pm(\alpha/\pi)^2$.

A weakness in the existing analysis is the assumed sharp high-energy cutoff that leads to the upper limit of 2π in the integration in Eq. (33). The value of this cutoff was constrained in the previous section by the $(\alpha Z)^2$ dependence of the magnetic moment of bound electrons. The second-order nature of the diagram used to obtain our picture of the magnetism of electrons (see Fig. 8) means that higher-order effects have not been constrained by the analysis in the preceding section, and thus we need to consider the possibility that the upper limit in the integration in Eq. (33) has a relative uncertainty of $\sim\alpha/\pi$.

It is likely that the direction-reversing emission mentioned above will not occur with exactly unit probability (even in the case of non-accelerating particles). Without further analysis, we suggest it is not unreasonable that the probability of the direction-reversed photon emission following an exchange could be a value as low as $1-\alpha/\pi$. To cover a possible range from unity to the suggested lower limit in the preceding sentence, we assume a direction-reversed photon emission probability of $1-(1\pm1)\alpha/2\pi$.

Incorporating the above discussions we rewrite Eq. (33) as

$$\alpha = \frac{1+\alpha/2\pi\pm(\alpha/\pi)^2}{2\pi}\int_0^{2\pi(1\pm\alpha/\pi)}\frac{[1-\exp(-\varepsilon^2/2\pi)]^2}{[\exp(\varepsilon)-1+(1\pm1)\alpha/2\pi\,]}\frac{d\varepsilon}{\varepsilon}\,. \qquad (35)$$

The corresponding solution is $\alpha = 1/137.06(2)$ with a universal charge of $e = 1.6020(2)\times10^{-19}$ C. The uncertainty estimate is dominated by the assumed uncertainty in the probability of the direction-reversed photon emission following an exchange. Additional work is needed to justify (or negate) the inclusion of the α/π related terms in Eq. (35).

Some will believe that, without a strong theoretical backing for the modifications suggested in this subsection, the favorable result obtained using Eq. (35) must be viewed as being fortuitous. However, I believe the reason for the numerical value of the fine-structure constant is such a longer standing and central mystery, there is a place for some educated guessing. Only additional studies of higher-order effects within the proposed black hole inspired photon-particle interaction mechanisms will be able to distinguish between breakthrough or fortuitous result. This is likely to be a long and laborious task, beyond the scope of the present study. I remind the reader that after the development of QED, it took eight years to get $g/2$ to fourth order [34] and an additional thirty-nine years to get it to sixth order [35]. Here I have tried a short-cut to obtaining some of the higher-order corrections needed to obtain an accurate result for α, within the proposed frame work, by assuming a connection between our desired higher-order corrections and the well-studied case of the electron's magnetic moment. We humbly suggest that a detailed study of long-wave-length stimulated emission induced by photon exchanges between a pair of small black holes might be a fruitful course of action.

VIII. Larmor emission

In the previous section, we used a mechanism where charge might be an emergent property associated with the exchange of stimulated-virtual photons between a pair of point particles. A value near the universal charge is obtained by imagining a direction-reversing stimulated-emission process that causes virtual photons to "rattle" between a particle pair. In this speculative model a particle can initiate a photon exchange which "jumps" across the separation distance d in a time of d/c. Previously, a weak interaction between an electron pair (at large separation distances) was invoked, where the acceleration of the particles could be ignored with the direction-reversed emission assumed to be projected back into the

source particle with a jump probability controlled by the time-energy uncertainty principle and higher-order corrections. This would require the particle pair and the exchanging photon(s) to be in some sort of entangled state where the direction-reversing stimulated-emission process "knows" which direction to send the emitted photon, so it "automatically" finds the partner particle. It is possible that such a process might be nearly perfect if both particles are stationary in non-accelerating inertial frames, but would likely need modification in the case of accelerating particles. Such a modification might lead to some of the stimulated-virtual photon exchanging energy being scattered (or absorbed and re-emitted) to infinity as real photons. If true, this would be a new and novel mechanism for Larmor emission that does not require the addition of a radiation resistance associated with an electron's self-interaction. Here we explore the possibility that, in the case of accelerating particles, there is a mismatch in the returning exchanged photon's sizes, as seen by the particle, relative to those associated with the "automatic" reabsorption in the case of non-accelerating particles. This mechanism is used here to obtain a result close to the Larmor formula for the power of electromagnetic emission from an accelerating electron.

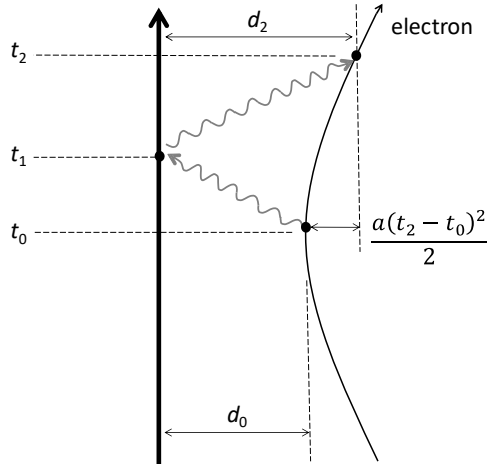

Fig. 15. A depiction of double photon exchange near the electron's turning point relative to a massive charged particle (see text). The bold line represents the stationary massive particle moving through time.

To simplify the calculation of the effects of a classical-like smooth acceleration a of a single electron, (with mass m), we place a massive point charge a distance $d_0=[\alpha\hbar c/(ma)]^{1/2}$ from the electron with the same velocity as the accelerating electron at $t_0=0$, and then view this process in the rest frame of the massive particle. Fig. 15 is a Feynman-like diagram that depicts a double photon exchange between the massive charged particle and the electron. We assume the accelerating electron initiates an exchange with the massive particle at $t_0=0$. This exchange takes a time $t_1=d_0/c$, and could be initiated by either a vacuum-virtual photon or a stimulated-virtual photon making an exchange from the massive particle to the electron. If there was no acceleration, the return time of the direction-reversed stimulated emission, t_2-t_1, back to the electron, would be the same. However, the acceleration increases this time to (see appendix A)

$$t_2 - t_1 = \frac{d_0}{c}(1 + 2\beta + 4\beta^2), \tag{36}$$

to second order, where $\beta=ad_0/c^2$. The corresponding square of d_0 relative to the return distance d_2 is (see Appendix A)

$$\left(\frac{d_0}{d_2}\right)^2 = 1 - 4\beta + 4\beta^2\,. \tag{37}$$

This factor is the relative change in the angular size of the electron as viewed from the origination site of the direction-reversed emission, relative to the case of a non-accelerating electron.

At the time of absorption at the end of the double exchange depicted in Fig. 15, the accelerating particle is moving with a speed of $v_2/c=2\beta+2\beta^2$ (see appendix A). Due to the corresponding Doppler shift, the effective reduced wavelength of the absorbed photon relative to its original value is (see appendix A)

$$\left(\frac{\lambda\!\!\!^{-}_2}{\lambda\!\!\!^{-}_0}\right)^2 = 1 + 4\beta + 4\beta^2 \tag{38}$$

to second order (including relativistic effects). This factor is the relative change in the size of the direction-reversed photons as viewed by the electron, relative to the case of a non-accelerating electron. Combining Eq.s (37) and (38) gives a relative change in the photon-electron effective interaction size, relative to the case of a non-accelerating electron of (see Appendix A)

$$\left(\frac{\lambda\!\!\!^{-}_2}{\lambda\!\!\!^{-}_0}\frac{d_0}{d_2}\right)^2 = 1 - 8\beta^2. \tag{39}$$

Notice that to first order the increase in the separation distance cancels with the increase in the exchanging photon's wavelength as seen by the electron. However, to second order the acceleration reduces the relative effective size of the direction-reversed-photon electron interaction by $8\beta^2$. We assume this effective interaction size change causes $8\beta^2$ of the direction-reversed photon energy to be scattered towards infinity as "real" emission.

The second-order force from Eq. (32), which includes the direction-reversed stimulated emission, can be rewritten as

$$F\sim\frac{\hbar c}{2\pi d^2}\int_0^{2\pi}\left\{1-\exp\left(-\frac{\varepsilon^2}{2\pi}\right)\right\}^2\frac{1-\exp(-\varepsilon)+\exp(-\varepsilon)}{[\exp(\varepsilon)-1]}\frac{d\varepsilon}{\varepsilon}=\frac{\alpha\hbar c}{d^2}. \tag{40}$$

The positive and negative $\exp(-\varepsilon)$ terms in Eq. (40) cancel, and were thus not included in the earlier version given in Eq. (32). However, these terms are now needed, with the $1-\exp(-\varepsilon)$ term being due to the first (initial) exchanges, while the $\exp(-\varepsilon)$ term is associated with the direction-reversed exchanges that can be influenced by the acceleration of the particles. The corresponding electromagnetic power being exchanged from the massive charge to the accelerating electron can be expressed as

$$P\sim\frac{\hbar c^2}{4\pi d^2}\int_0^{2\pi}\left\{1-\exp\left(-\frac{\varepsilon^2}{2\pi}\right)\right\}^2\frac{1-\exp(-\varepsilon)+\exp(-\varepsilon)}{[\exp(\varepsilon)-1]}\frac{d\varepsilon}{\varepsilon}. \tag{41}$$

Given the assumptions associated with Eq. (39), the corresponding power associated with the conversion of the direction-reversed stimulated-virtual-photon energy into real emission is given by

$$\begin{aligned}P\sim&\frac{\hbar c^2}{d^2}\frac{8\beta^2}{4\pi}\int_0^{2\pi}\left\{1-\exp\left(-\frac{\varepsilon^2}{2\pi}\right)\right\}^2\frac{\exp(-\varepsilon)}{[\exp(\varepsilon)-1]}\frac{d\varepsilon}{\varepsilon}\\ =&\frac{2}{\pi}\int_0^{2\pi}\left\{1-\exp\left(-\frac{\varepsilon^2}{2\pi}\right)\right\}^2\frac{\exp(-\varepsilon)}{[\exp(\varepsilon)-1]}\frac{d\varepsilon}{\varepsilon}\;\;a^2\frac{\hbar}{c^2}\\ =&\;0.005003\ldots a^2\frac{\hbar}{c^2}\sim 1.028\ldots\frac{2}{3}\alpha a^2\frac{\hbar}{c^2}\;.\end{aligned} \tag{42}$$

This result is ~3.0% higher than the Larmor formula and is perhaps close enough that higher-order effects might be capable of reducing the pre-factor of 1.028… on the RHS of Eq. (42) to a value much closer to unity. The ability to construct this new picture of Larmor emission adds some credibility to the photon rattling process used to obtain an estimate of the fine-structure constant in the previous section. We note that introducing the higher-order correction terms used to obtain Eq. (35) along with an additional scaling term of $1/(1+4\alpha)$ of unknown origin, gives

$$P=\frac{a^2\hbar}{c^2}\frac{2}{\pi}\frac{(1+\alpha/2\pi)}{1+4\alpha}\int_0^{2\pi}\left\{1-\exp\left(-\frac{\varepsilon^2}{2\pi}\right)\right\}^2\frac{\exp(-\varepsilon)}{[\exp(\varepsilon)-1+(1\pm1)\alpha/2\pi]}\frac{d\varepsilon}{\varepsilon} \tag{43}$$

with the favorable result of $P = 0.6666(2)\cdot\alpha a^2\hbar/c^2$, where here α is assumed to be as given by Eq. (35). It is unclear if this result is an indication of the true nature of the higher-order corrections that need to be applied to Eq. (42), or a highly fortuitous result. We speculate that the higher-order correction associated with the $1/(1+4\alpha)$ term is due to some re-absorption of the initial Larmor emission by the particle pair. We humbly suggest the a detailed study of stimulated emission induced by a photon exchange between a pair of accelerating black holes might be a fruitful course of action.

An area of difficulty in electrodynamics has been the conservation of energy in the presence of Larmor emissions. The problem occurs because the force that generates the initial electron acceleration conserves energy locally; i.e. the work done by the applied force goes into changing the state of the electron. However, the associated Larmor emissions to infinity then violate conservation of energy, unless a radiation resistance is applied to the accelerating electron. This can be done by invoking the second term in the electron's self-reaction force as first determined by Lorentz [36]. In the model presented here, the charge of an electron is an emergent property associated with the whole electron, and there is no mechanism for subdividing the electron into subunits which can interact with each other in the manner used by Lorentz. However, the Larmor emission mechanism suggested here does not need a radiation resistance. Instead, the scattering of some of the exchanging photon energy to infinity can conserve energy by reducing the acceleration associated with the exchanging photons.

IX. Vacuum polarization

We have invoked a picture where electrons are chargeless black holes that can exchange virtual photons via emission properties that are not dissimilar to Hawking radiation. With the inclusion of various speculative model choices the photon exchanges between, and the self-absorption by, chargeless black-hole-like objects can be made to deliver many of the properties of electromagnetism at length scales larger than the reduced Compton wavelength. However, the above picture with only photon exchanges is inconsistent with the known effects of vacuum polarization [19], which cause the electric field around a charged particle to be larger than the nominal inverse square law result (without vacuum polarization) at short length scales. This effect can be visualized as in Fig. 16 where a highly charged "naked" electron repels and attracts virtual electrons and positrons, respectively. Within this picture, the highly charged naked electron is screened by the vacuum polarization such that it appears to have the fundamental unit of charge if observed on length scales larger than the reduced Compton wavelength, $\lambda\!\!\!^{-}_C$. For observations on shorter length scales the seeable charge of the electron grows logarithmically toward infinity as the length scale approaches zero. This is the reason for renormalization and the running of the coupling constant in QED.

The apparent dependence of an electron's effective charge on the observational length scale can be used to discredit the idea of a universal charge via the theory represented by Eq.s (33) and (35). However, there is a way around this issue. At high black-hole temperatures, Hawking radiation includes particle emission along with photon emission. Therefore, if electromagnetism at large length scales is due to the emission and absorption of virtual photons generated by a Hawking-radiation-like emission process, then the exchange of electrons should generate effects at length scales less than a few $\lambda\!\!\!^{-}_C$, where the exchange temperature is comparable to or larger than the rest-mass energy of an electron. Given this, in this section, we explore a new picture of vacuum polarization where electrons can be evaporated from a real particle and absorbed by a nearby real partner particle. However, it is useful to first summarize the effects of vacuum polarization from standard theory.

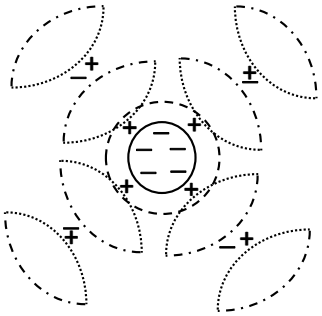

Fig. 16. Schematic representation of vacuum polarization. The dashed circle represents a spherical surface with a radius of $\lambda\!\!\!^{-}_C$ about the center of a real electron. The dashed-dotted and dashed arcs represent polarized virtual electron-positron pairs surrounding the real electron. From outside this dashed circle the electron appears to have the fundamental charge *e*. At length scales $d < \lambda\!\!\!^{-}_C$, the apparent (or effective) charge is larger, growing logarithmically towards infinity as *d* approaches zero.

The definitive paper on the potentials induced by vacuum polarization in the case of static fields is still the one by Uehling [19] published in 1935. In this seminal paper, Uehling shows that the modification of the electrostatic potential between two unit charges, associated with the polarization of the vacuum, is given by

$$\frac{\Delta \mathrm{V}(r)}{\mathrm{V}_0(r)} = \frac{\alpha}{\pi}\int_0^1 (1-u^2)\int_1^\infty \exp\left(\frac{-2rz}{\sqrt{1-u^2}}\right) dz\, du\,, \tag{44}$$

where $\mathrm{V}_0(r)$ is the nominal potential without vacuum polarization, and *r* is in units of $\lambda\!\!\!^{-}_C$. In the same paper, Uehling also showed that the corresponding limits can be given by

$$\lim_{r\to\infty}\left(\frac{\Delta \mathrm{V}(r)}{\mathrm{V}_0(r)}\right) = \frac{\alpha}{4}\frac{\exp(-2r)}{\sqrt{\pi}\cdot r^{3/2}}, \quad \text{and} \tag{45}$$

$$\lim_{r\to 0}\left(\frac{\Delta \mathrm{V}(r)}{\mathrm{V}_0(r)}\right) = -\frac{2\alpha}{3\pi}\left[\gamma + \ln(r) + \frac{5}{6}\right], \tag{46}$$

where γ=0.5772… is Euler's constant. Eq.s (44) to (46) are displayed in Fig. 17. Please notice that the vacuum polarization corrections are relatively small, being less than one part in 10^4 at a distance of $\lambda\!\!\!^{-}_C$, and are still less than 1% at one hundredth of a reduced Compton wavelength (~3 fm). However, these changes deliver measurable modifications to electronic based Lamb shifts and dominate the Lamb shifts of muonic atoms [37,38]. Also notice that the large length approximation given by Eq. (45) approaches Eq. (44) slowly, and is not a good representation of the full result until *r* is much larger than ten where the vacuum polarization is infinitesimally small. Eq. (46) does not accurately represent the full result until *r* is less than ~0.05. This small length scale does not significantly contribute to the measurable Lamb shifts of light atoms because the corresponding electrons spend very little time at such short distances. This means that Eq.s (45) and (46), although interesting and useful for testing numerical methods for evaluating Eq. (44), are not directly useful in determining Lamb shifts.

The shift in atomic energy levels associated with vacuum polarization can be estimated using

$$\Delta E = \int_0^\infty \Delta \mathrm{V}(r)|\psi_{nl}(r)|^2 4\pi r^2 dr \tag{47}$$

where $\Delta \mathrm{V}(r)$ is the modification of the potential obtainable using Eq. (44). If the radial dependence of the central region of the 2*s* hydrogen wave function is ignored and the nuclear mass is assumed to be infinite (close to reality for light electronic systems) then it is straightforward to obtain the analytical result of

$$\Delta E_{2s} = \frac{\alpha^5 mc^2}{30\pi} = 27.129 \text{ MHz (for electronic hydrogen)} \tag{48}$$

for the vacuum polarization contribution to the corresponding Lamb shift [19]. This is a convenient result to test the accuracy of numerical methods used to solve Eq.s (44) and (47). The change in the potential energy associated with vacuum polarization, $\Delta V(r)$, can be obtained by multiplying the relative change given by Eq. (44) by $V_0 = \alpha\hbar c/d$. Therefore, including the $4\pi r^2 dr$ volume element, a key step in the path to evaluating Eq. (47), for electronic hydrogen *s*-state systems where the wave function length scale is much larger than $\lambda\!\!\!^{-}_C$, is Eq. (44) multiplied by *r*. The importance of different radii to the electronic hydrogen *s*-state vacuum-polarization Lamb shift components is illustrated by the product of Eq. (44) with *r* in Fig. 18 (dotted curve). Notice that this function peaks at $r \sim 0.2$, with approximately one half of its integral due to $r < 1/2$, and with little contribution from $r > 2$.

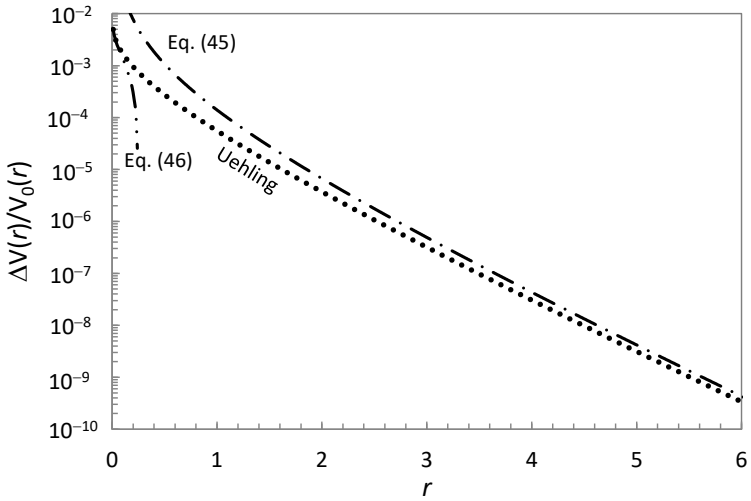

Fig. 17. Estimates of the potential change due to vacuum polarization: full calculation via Eq. (44) (Uehling, dotted curve); the large distance approximation via Eq. (45) (dash-dotted curve); and the short distance approximation via Eq. (46) (dash-double-dotted curve). The length (radius) *r* is in units of $\lambda\!\!\!^{-}_C$.

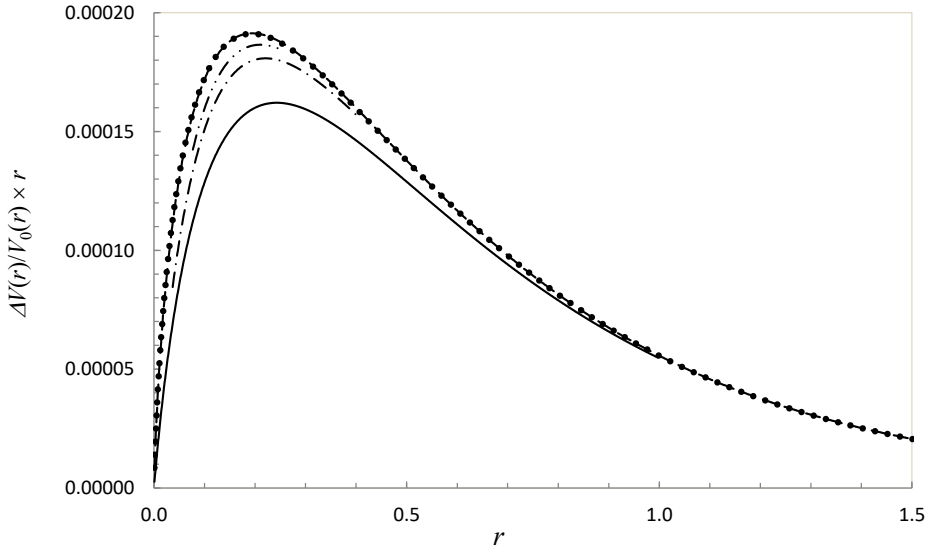

Fig. 18. Eq. (44) multiplied by *r* (dotted curve, which may be difficult to make out because it coincides with the dashed curve). This illustrates the relative importance of different radii to the calculation of electronic hydrogen *s*-state vacuum-polarization Lamb shift components. The other curves are obtained using the black hole (electron) exchange model introduced in this paper: single black hole (electron) exchanges (solid curve); single and double exchanges (dash-dotted curve); single, double, and triple exchanges (dash-double-dotted curve); and including all exchange types (dashed curve).

IX.A Exchange of virtual electrons between a real electron pair

To exploring a new picture of vacuum polarization, we start with Eq. (32), and introduce the idea that a pair of real electrons can exchange an electron via an evaporation-like process. This statement appears absurd at first, because it violates conservation of charge at both the emission and absorption sites. However, assuming charge is an emergent property of an interaction mechanism, the idea that a chargeless black hole evaporates another chargeless black hole which is then absorbed by a different nearby chargeless black hole does not seem completely unreasonable. Here, we show that a force between two real electrons can be obtained via the above mentioned particle exchange mechanism, and this force can be made to look remarkably like vacuum polarization at length scales larger than $\lambda\!\!\!^{-}_C$. The inclusion of additional assumptions regarding the exchange of more complex entities (see the following subsection) can deliver a force (and potential) that is very close to that of Uehling vacuum polarization at length scales down to a small fraction of $\lambda\!\!\!^{-}_C$. This model is used to estimate its effects on the Lamb shift of hydrogen, and muonic hydrogen and deuterium. These results are close to the corresponding effect of vacuum polarization, and suggest that there might be a different way of visualizing this process.

In analogy to the force generated by the exchange of virtual photons [see Eq. (32)], the exchange of virtual electrons between a pair of real electrons might be expected to generate a force of the form

$$F_1 = 2\,\frac{1}{2\pi}\int_0^{\pi\hbar c/d} T^2(\alpha,d)\exp(-mc^2/T_{\rm ex})\frac{(1-\exp(-2d^2/\pi\lambda\!\!\!^{-2}_0))^2}{[\exp(\varepsilon/T_{\rm ex})+1]}\frac{d\varepsilon}{\pi\hbar}p\frac{\pi\lambda\!\!\!^{-2}}{d^2}. \qquad (49)$$

The exchanging electrons with a rest-mass energy of mc^2 are spin ½ Fermions, and thus the modification of the Planckian exponential minus 1 term to an exponential plus 1 [15,39]. Being spin ½ Fermions, the exchanging particles have two helicity states, similar to the massless spin-1 photons. There is thus no overall scaling factor change associated with a change in the number of possible helicity states. The $\exp(-mc^2/T_{\rm ex})$ term is a phase-space reduction factor associated with the rest-mass energy of the exchanged particle relative to the corresponding effective temperature. We assume that at and soon after the initial evaporation, the exchanging virtual electron has not yet existed for long enough as a separate entity to have built up its own virtual photon cloud, and thus behaves as a massless (or near massless) particle. By time reversal symmetry the same must apply at absorption. Therefore, for near-field virtual-electron emission and absorption purposes we assume the relevant wave length is $\lambda\!\!\!^{-}_0=\hbar c/\varepsilon$, where ε is the energy of the particle at evaporation, and is the energy in excess of its rest-mass energy in midflight. On the time scale of the initial evaporation process, we assume that the system cannot tell which massless black hole is the evaporated object and which one is the parent object. This doubles the probability that a single black hole (particle) is sent in the required direction to be reabsorbed by the real partner particle and is the reason for the factor of "2" out the front of Eq. (49). The momentum p of the exchanging particle after it transitions to full mass (midflight) can be expressed as $(\varepsilon+mc^2)^2=(pc)^2+(mc^2)^2$ and thus

$$\lambda\!\!\!^{-} = \frac{\hbar c}{\varepsilon\sqrt{1+2mc^2/\varepsilon}}. \qquad (50)$$

The $T(\alpha,d)$ term is a transmission coefficient associated with the quantum tunneling of the virtual electron through the electromagnetic potentials surrounding the real electrons that make up the exchanging pair [40,41]. For a macroscopic daughter black hole of unit negative charge evaporating an electron, the transmission coefficient is [41]

$$T(\alpha) = \exp(-\alpha\hbar c/r_S T_{\rm bh}). \qquad (51)$$

There are strong parallels with proton emission from hot nuclei where the decay width is proportional to $\exp(-\Delta E/T)\cdot\exp(-\alpha Z\hbar c/r_B T)$ [42] where ΔE is the proton binding energy, Z and T are the atomic number and temperature of the daughter nucleus, and r_B is the Coulomb-barrier radius which is approximately the

daughter radius plus the range of the nuclear force. However, there is no corresponding theory for the emission of electrons from very small black holes. As discussed before, the idea that a small black hole can contain an effective length scale that is orders of magnitude smaller that the Planck length makes no physical sense, and the required relevant barrier radius is more likely controlled by quantum physics, and not by the gravitation constant G. In the case of two interacting real electrons separated by a distance d, we will soon demonstrate that we can gain a favorable result by assuming that the evaporating virtual electrons need to be separated from the parent particle (black hole) by a distance $r_B = 2\alpha d/\pi$ before they can be viewed by the electromagnetic vacuum as a separate entity. This has parallels with the near-field effects introduced in section VI, but on a length scale ~1/137 times smaller. The emission barrier corresponding to the above assumption, for our two real electron system, is $V_B \sim \alpha\hbar c/r_B + \alpha\hbar c/d$. It seems logical to assume that the relevant temperature will be $T_{ex} = \hbar c/2d$ and rewrite Eq. (51) as $T(\alpha) \sim \exp(-\pi - 2\alpha)$. Including these considerations, and reintroducing the same scaling used to obtained Eq.s (35) and (43); and switching to an ε in units of T_{ex}, leads to the result

$$F_1 = \frac{\alpha\hbar c}{d^2}\left(1+\frac{\alpha}{2\pi}\right)\frac{\exp(-2\pi-4\alpha)}{\pi\alpha}\exp\left(\frac{-2d}{\lambda\!\!\!^{-}_C}\right)\int_0^{2\pi}\frac{(1-\exp(-\varepsilon^2/2\pi))^2}{[\exp(\varepsilon)+1]\sqrt{1+4d/\varepsilon\lambda\!\!\!^{-}_C}}\frac{d\varepsilon}{\varepsilon}. \qquad (52)$$

Switching d into r (in units of $\lambda\!\!\!^{-}_C$) gives the force due to electron exchanges relative to the photon exchanges as

$$\frac{F_1}{F_0} = \left(1+\frac{\alpha}{2\pi}\right)\frac{\exp(-2(\pi+r+2\alpha))}{\pi\alpha}\int_0^{2\pi}\frac{(1-\exp(-\varepsilon^2/2\pi))^2}{[\exp(\varepsilon)+1]\sqrt{1+4r/\varepsilon}}\frac{d\varepsilon}{\varepsilon}. \qquad (53)$$

Some of the factors that make up Eq.s (53) and (35) are summarized in Fig. 19. A stepwise representation of Fig. 19(a) is given in Fig. 20.

Even the classical evaporation of charged particles is made very complex by the presence of a third nearby particle, as evidenced by the study of ternary fission [43], particularly in the case of a dynamically evolving system like a fissioning nucleus or two closely-spaced real electrons. We cannot hope here to solve the many body problem that is the exchange of a black hole between a black hole pair, where the exchanging black hole continues to interact with the real pair during the exchange. However, we now proceed with scoping calculations that hopefully illustrate some of the complexity of what will need to be addressed in a more complete theory. Notice that in Fig. 19(a) we have no higher-order corrections associated with the exchanging electron's midflight interaction with the real electron pair via photon exchange. A Feynman-like diagram to illustrate this effect is presented in Fig. 21. Notice that the virtual electron is assumed to be born and absorbed with no mass, travelling at the speed of light. The electric potential of the exchanging electron along the straight line path between the two real electrons is displayed in Fig. 22. We can use Fig. 22 to place limits on the transmission coefficient $T(\alpha)$. If the interaction potential was equal to the minimum value displayed in Fig. 22, at all locations, then the energy required to generate an exchange would be $8\alpha T_{ex}$ higher than mc^2. This would diminish the exchanges by a factor of $\exp(-8\alpha)$ with a corresponding effective transmission coefficient of $\exp(-4\alpha)$. This value is larger than the required true value of $T(\alpha)$. Scaling the potential, from only one of the exchanging electrons, by $(1+2\alpha/\pi)$ increases the barrier to the required height but underestimates the required potential in the mid-flight region (see dashed black curve in Fig. 22). We thus know that the required transmission coefficient must be less than $\exp(-\pi-2\alpha)$. Adding a constant of $4\alpha T_{ex}$ to the potential from only one of the exchanging particles gives the correct midpoint potential but overestimates the potential as we move towards the chosen particle (see dotted curve in Fig. 22), and thus we suspect that $T(\alpha) > \exp(-\pi-4\alpha)$. To model the electron exchange correctly one should include more than the potential along a straight line path between the two exchanging electrons, because the exchanging particle's wave-like properties smear

out its location, and allows for non-straight line paths. Fig. 23 displays a contour plot of the axially symmetric potential generated by the two exchanging real electrons and a possible non-straight-line path for the exchanging particle. Without this consideration one would lean towards the lower limit of $\exp(-\pi -4\alpha)$ for the transmission coefficient. However, the lower mid-flight potentials available to the exchanging particle (see Fig. 23) favor a higher transmission coefficient more towards the middle of the above discussed limits, leading to the expectation of $T(\alpha) = \exp(-\pi-(3\pm\Delta)\alpha)$ with the uncertainty $\Delta < 1$. The value of $3\pm\Delta$ will be refined in the next subsection. Including the above update to $T(\alpha)$ modifies Eq. (53) to

$$\frac{F_1}{F_0} = (1+\frac{\alpha}{2\pi})\frac{\exp(-2(\pi + r + (3 \pm \Delta)\alpha))}{\pi\alpha}\int_0^{2\pi}\frac{(1-\exp(-\varepsilon^2/2\pi))^2}{[\exp(\varepsilon)+1]\sqrt{1+4r/\varepsilon}}\frac{d\varepsilon}{\varepsilon}. \qquad (54)$$

We acknowledge that several of the assumptions used to obtain Eq. (54) are unorthodox, but proceed with a comparison to Uehling.

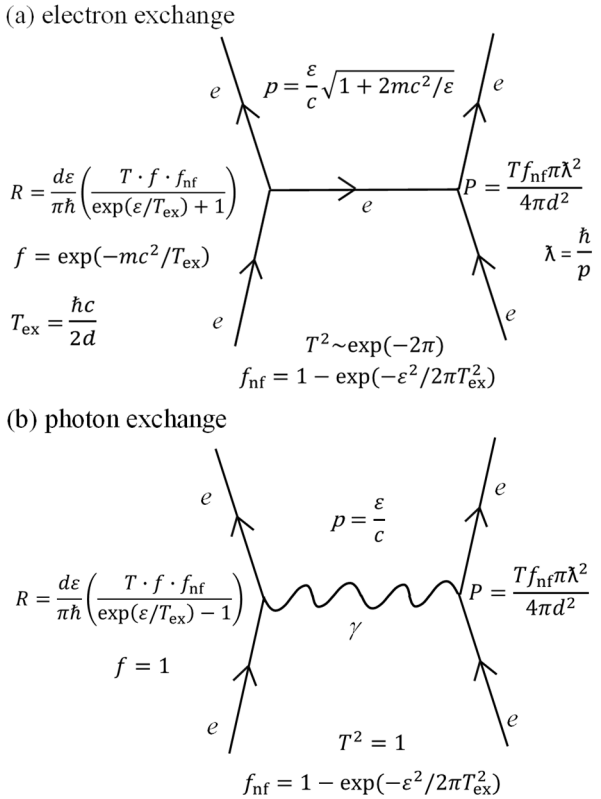

Fig. 19. A summary of some of the factors contained within Eq.s (53) and (35), for (a) electron and (b) photon exchanges. The effective exchange-particle emission rate, R, is shown on the left with the corresponding absorption probability, P, on the right. The momentum of the exchanging particle, p; the assumed near-field correction, $f_{\rm nf}$; and the transmission coefficient squared are displayed between the real particle pairs.

Solving for the force given by Eq. (54) (with Δ=0), as a function of r, and integrating it inwards from infinity gives the potential (V_1) depicted by the solid curve in Fig. 24. Please notice the excellent agreement with the vacuum polarization result from Uehling for length scales larger than $\lambda\!\!\!^{-}_C$. If the potential corresponding to Eq. (54) were displayed in Fig. 17 the differences from Uehling would be barely visible to the eye. This result supports the choice that, in the case of two interacting particles separated by a distance d, the evaporating virtual electrons need to be separated from the parent particle (black hole) by a distance $r_B = 2\alpha d/\pi$ before it can be viewed by the electromagnetic vacuum as a separate entity, and suggests a possible connection between vacuum polarization and the picture presented here

where the electromagnetic force between two electrons is generated by the exchange of both photons and electrons. In the region from $r = 1.5$ to 7, the rms difference between Uehling and the present model is about two parts per thousand (i.e. $\sim\alpha/\pi$). The absolute agreement is obtained by the empirically determined barrier radius discussed above, and is not the main interesting result. It is the agreement in the radial dependence of the two models at $r > 1$ over more than six orders of magnitude in $\Delta V/V_0$ that is difficult to dismiss as a fortuitous coincidence. At a minimum, this result suggests a closer inspection is warranted.

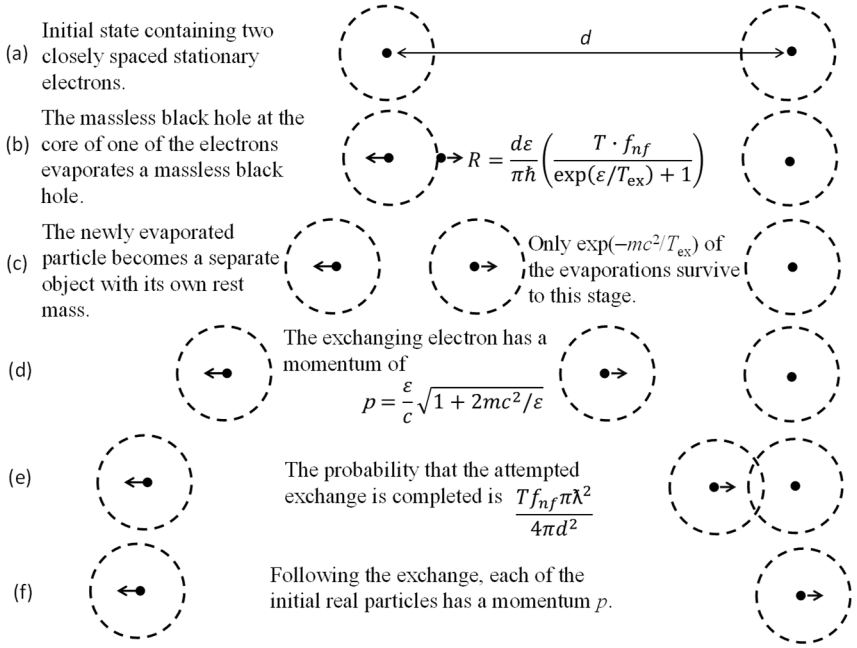

Fig. 20. A stepwise representation (a-f) of an electron exchange between a pair of real particles corresponding to the exchange displayed in Fig. 19(a). The dashed circles represent an effective minimum size of interacting black holes. As discussed in the text, the effective minimum size is much smaller than depicted here.

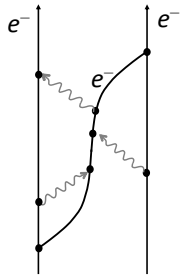

Fig. 21. A depiction of an exchanging electron that interacts via photon exchange, during the midflight region, with the emitting and absorbing real particle pair.

As presented in Fig. 24, the difference between the Uehling vacuum polarization potential change (dotted curve) and the corresponding result using the single electron-exchange model (solid curve) at $r <$ 1.0 may, at first, appear small. However, as demonstrated in Fig. 18, the corresponding Lamb shift components are dominated by the vacuum polarization within a distance of $\lambda\!\!\!^{-}_C$, with the peak in the relative potential change $\times$ r being near $r \sim 0.2$. The corresponding relative potential change $\times$ r for the single electron-exchange model is displayed by the solid curve in Fig. 18. The comparison between the dotted and solid curves in Fig. 18 is a better way of comparing Uehling and the single electron-exchange model presented here, at least in relation to Lamb shift components due to vacuum polarization. The corresponding Lamb shift components for the single electron-exchange model are presented in Table II.

These are 10-20% lower than the corresponding values from Uehling. This difference is due to the growing discrepancy between the Uehling potential change due to vacuum polarization (dotted curve in Fig. 24) and Eq. (54) (solid curve in Fig. 24) at short length scales. The possibility that this discrepancy is due to the exchange of more complex entities is discussed in a following subsection.

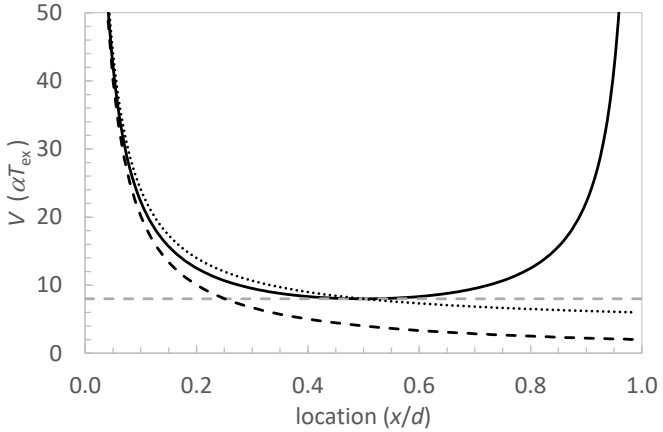

Fig. 22. The electric potential of an exchanging electron along the straight line path between the two real electrons in units of αT_{ex} (solid curve). The horizontal dashed gray line shows the minimum at $8\alpha T_{ex}$. The potential from just one of the exchanging pair scaled by $1+2\alpha/\pi$ is displayed by the dashed black curve. The dotted curve is the potential due to a single particle plus $4\alpha T_{ex}$ (see text).

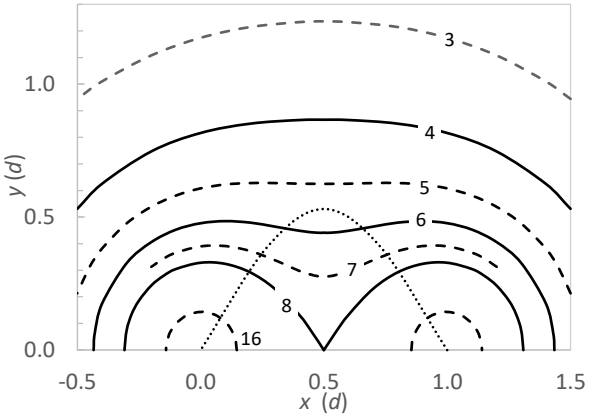

Fig. 23. Contour plot of the axially symmetric potential (solid and dashed curves) felt by an exchanging unit charge. The potential contours are in units of αT_{ex}. The dotted line indicates a possible non-straight path for a given exchange.

Table II. The Lamb shift components of: the 2*s* hydrogen state, ignoring the radial dependence of the electron's wave function with an infinite mass proton; and the non-relativistic 2*s*-to-2*p* muonic hydrogen and deuterium atoms including the corresponding radial dependence of their wave functions and the finite mass of the nuclei, due to the electron-exchange model presented here, and the corresponding Uehling calculations reported in the literature [19,37,38]. The exchange of electron clusters is discussed in the next subsection.

Energy shifts due to vacuum polarization	2*s* electronic (MHz)	2*s*-to-2*p* muonic(meV)	
	hydrogen	hydrogen	deuterium
single electron exchanges	24.47	166.4	183.8
including double exchanges	26.16	187.4	207.4
including triple exchanges	26.61	194.5	215.4
including all exchanges[a]	27.13±0.04	204.7±0.3	227.2±0.3
Uehling	27.129	205.0	227.6

[a] Uncertainties assuming Δ=0.2, see Eq. (57) and the discussion regarding Fig. 26 in the next subsection.

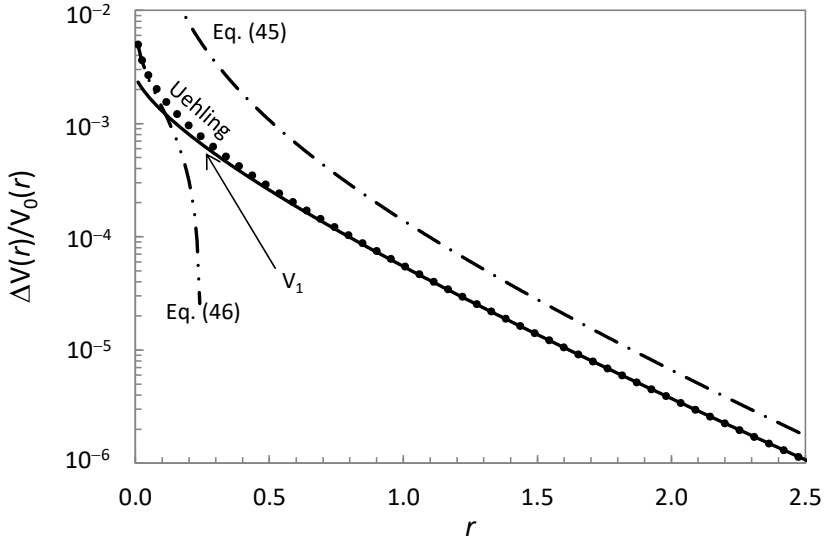

Fig. 24. As for Fig. 17, but on a smaller length scale, and with the addition of the potential associated with the exchange of single electrons (V_1, solid curve) via the force given by Eq. (54).

IX.B Exchange of more complex entities between a real electron pair

Due to quantum effects, many particle emission processes do not emit a simple stream of uncorrelated single particles, but instead emit particles in correlated clusters. The Hanbury Brown and Twiss effect [44,45] is an example of this for photon sources. Here, we assume something similar occurs in the electron-exchange mechanism introduced in the previous subsection. No theory exists to help with the nature of such a process, so we instead assume that QED can be viewed via both the standard field-based description and a new black-hole particle-based description, and that these two pictures give identical (or near identical) results. With this assumption, we can infer complex black-hole and electron emission processes that give results close to standard theory. The following is a discussion of model choices for the evaporation of correlated black-hole entities that succeed in giving a near equivalence between standard vacuum polarization and the presented model.

As discussed in the previous subsection, we accept that in the case of two interacting real small black holes separated by a distance d, there is an effect that places a lower limit of $2\alpha d/\pi$ on the size of the real black holes and any exchanging black-hole related entities. This limit can be viewed as a substitute for the Schwarzschild radius, which becomes unphysically small for micro black holes. The physics of this limiting size may be related to the Lamb shift where the fuzziness of the electron-photon interactions is also a bit less than $1/137^{th}$ the characteristic size of the system. We imagine the evaporation of a correlated pair of black holes from a single black hole proceeds as depicted in Fig. 25. At first the evaporated pair (depicted by a pair of black dots joined by a bar) appears on the surface of the parent black hole. At this stage the newly formed black hole pair has not had time to interact with the electromagnetic vacuum outside the parent black hole and is thus assumed to initially behave as a massless spin-1 boson with two helicity states, like the photon. However, as viewed by the emitting and absorbing real particles, the initially evaporated massless black hole pair is a flat bar-like object with a twofold (180°) azimuthal symmetry (both black holes are assumed to be identical). This gives a twofold decrease in the azimuthal phase space relative to the case of single black hole emission. This drop in azimuthal phase space is assumed to drop the evaporation rate by a factor of two, relative to the case of a single black hole evaporation as presented in the previous subsection. In analogy with the case of photon evaporation, $1/2\pi$

of the initial boson emissions are assumed to be immediately self-absorbed. However, unlike the photon case, the small transmission coefficient means the vast majority of the self-absorptions are not followed by a re-emission. This causes a reduction of $\sim 1-1/2\pi$ in the evaporation rate of black-hole pairs relative to the photon case (higher-order corrections exist). After exiting from the parent, the black hole pair starts interacting with the electromagnetic vacuum outside the parent, and establishes its own identity with its own rest mass. Given that the black hole pair is contained within a space not directly accessible to the electromagnetic vacuum, the pair behaves as a single electromagnetic object with a single unit of charge but with twice the rest mass during the midflight region. In analogy to the case of single black hole evaporation, only a fraction $f = \exp(-2mc^2/T_{ex})$ of the black hole pairs survive the transition to full rest mass. The modification of Eq. (54), with the inclusion of these assumptions, gives the force associated with the exchange of black hole (electron) pairs between two real electrons as

$$\frac{F_2}{F_0} = (1-\frac{1}{2\pi})(1+\frac{\alpha}{2\pi})\frac{\exp(-2(\pi+jr+(3\pm\Delta)\alpha))}{2\pi j\alpha}\int_0^{2\pi}\frac{(1-\exp(-\varepsilon^2/2\pi))^2}{[\exp(\varepsilon)-1]\sqrt{1+4jr/\varepsilon}}\frac{d\varepsilon}{\varepsilon}, \qquad (55)$$

with the multiplicity of the exchanging clusters $j = 2$. The factor of two symmetry term from Eq.s (52) to (54) is removed because when evaporating a particle cluster, the system can tell the difference between the "single" black hole parent and the evaporated daughter object.

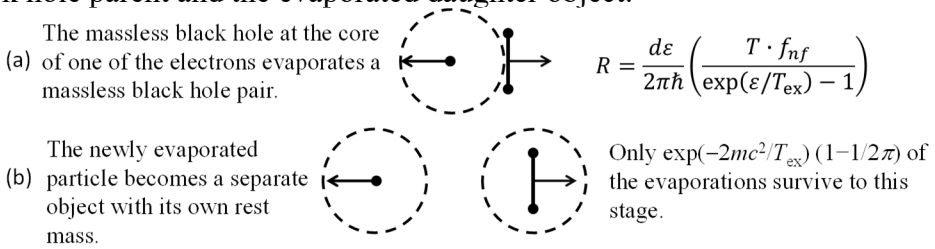

Fig. 25. The evaporation of a black hole pair from a parent black hole. In (a) the initially massless pair (depicted by a pair of black dots joined by a black bar) in born. By (b) the new pair has become a separate entity (see text).

Eq. (55) can be tested by comparing its consequences to Uehling minus V_1 (see Fig. 24). This is done in Fig. 26. V_i is the potential corresponding to the force F_i. If V_1 is correct then Uehling minus V_1 would contain the effect of all types of black hole exchanges with two, and possibly more, black holes (particles). The dotted and upper-black (V_1) curves (in Fig. 26) are the relative potential changes associated with vacuum polarization and single-electron exchanges, as displayed in Fig. 24. The solid black curve labelled V_2 displays the corresponding result using the force due to the exchange of black-hole pairs as given by Eq. (55). This should be compared to the dashed curve that is the difference between Uehling and V_1. Notice that V_2 and (Uehling minus V_1) approach each other as r increases beyond ~ 0.6. This is an extraordinary result because it tells us that V_1 approaches Uehling, with increasing r, in a manner where their small differences are close to V_2. This implies that at $r>0.6$ there is little contribution from exchanges containing more than two black holes. The difference between the V_2 and (Uehling minus V_1) at $r<0.6$ is perhaps due to the exchange of particle clusters containing three or more black holes. The dash-dotted curve in Fig. 18 shows the effect of including both single and double electron exchanges. The corresponding Lamb shift components are listed in Table II.

Continuing with the same logic, we assume clusters of three black holes behave as Fermions and can be exchanged in a manner similar to the pairs discussed above. The force due to the exchange of these triple clusters is

$$\frac{F_3}{F_0} = (1+\frac{\alpha}{2\pi})\frac{\exp(-2(\pi+jr+(3\pm\Delta)\alpha))}{2\pi j\alpha}\int_0^{2\pi}\frac{(1-\exp(-\varepsilon^2/2\pi))^2}{[\exp(\varepsilon)+1]\sqrt{1+4jr/\varepsilon}}\frac{d\varepsilon}{\varepsilon}, \qquad (56)$$

with the multiplicity of the exchanging clusters $j = 3$. This equation can be tested by comparing its consequences (V_3, solid curve in Fig. 26) to Uehling minus ($V_1 + V_2$) (dash-dotted curve). Notice that these curves appear to approach each other as r increases beyond ~0.5. This implies that at $r>0.5$ there is little contribution from exchanges containing more than three black holes. The difference between V_3 and Uehling minus ($V_1 + V_2$) at $r<0.5$ is likely due to the exchange of particle clusters containing four or more black holes. The dash-double-dotted curve in Fig. 18 shows the effect of including single, double, and triple black hole exchanges. Notice that the cluster-exchange picture is converging towards Uehling as the complexity of the exchanges is increased. The corresponding Lamb-shift components are listed in Table II, and are 2-5% lower than the corresponding correct values.

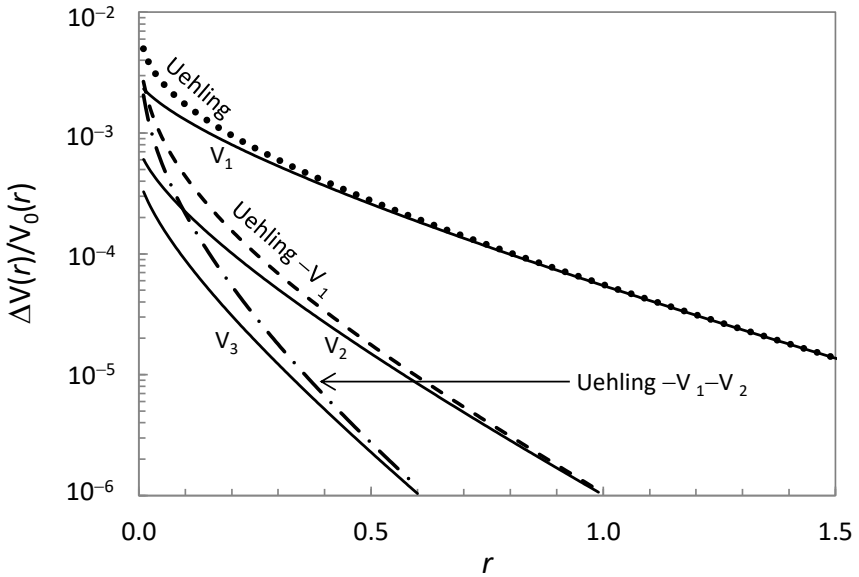

Fig. 26. Estimates of the potential change due to vacuum polarization: Uehling via Eq. (44) (dotted curve) and the corresponding result associated with the exchange of electron singles (V_1, solid curve); doubles (V_2, solid curve); and triples (V_3, solid curve) (all with $\Delta=0$). The dashed and dash-dotted dashed curves display the difference between Uehling and V_1, and Uehling and ($V_1 + V_2$), respectively. For an explanation of the importance of the dashed and dash-dashed curves, please see the text.

Please note that the comparison between the solid V_2 and V_3 curves and the difference curves (dashed and dash-dotted) in Fig. 26 becomes meaningless below $\Delta V/V_0 \sim 10^{-6}$, given that we suspect there are disagreements between Uehling and the presented model at about the two parts in a thousand level (i.e. with a relative difference of $\sim\alpha/\pi$). This causes the difference estimates in Fig. 26 (dashed and dash-dotted curves) to have large relative uncertainties when they are more than two-to-three orders of magnitude below the Uehling result. The favorable results displayed in Fig. 26 are obtained with Δ in Eq.s (54) to (56) set to zero. The results at and above $r = 0.5$ can be used to restrict Δ to be less than 0.2.

Following the above logic, we can express the force due to the exchange of clusters of j black holes as

$$\frac{F_j}{F_0} = S(1-P_{\rm sa})\left(1+\frac{\alpha}{2\pi}\right)\frac{\exp(-2(\pi + jr + (3\pm\Delta)\alpha))}{2\pi j\alpha}\int_0^{2\pi}\frac{(1-\exp(-\varepsilon^2/2\pi))^2}{[\exp(\varepsilon)\pm 1]\sqrt{1+4jr/\varepsilon}}\frac{d\varepsilon}{\varepsilon}, \qquad (57)$$

where S is 2 for single black-hole exchanges ($j=1$), and unity for all other exchange types; the probability of self-absorption is $P_{\rm sa}=1/2\pi$ for even j, otherwise zero; in the case of the $\pm$ sign the top symbol is for odd j (Fermions), and the bottom symbol for even j (Bosons). The force associated with photon exchange can be obtained by setting $T^2 = 1$, setting the $2\pi j$ term to 2π, all other js to zero, and $P_{\rm sa}$ to zero. The vacuum polarization force including all black-hole exchange types can be obtained by summing the F_j in

Eq. (57) over all j from 1 to ∞. The corresponding relative potential charge × r (dashed curve) is compared to the corresponding Uehling result (dotted curve) in Fig. 18. The rms difference between the relative potential differences between Uehling and the presented black hole cluster-exchange model is only α/π (two parts per thousand) across the range from r = 0.05 to 7. The corresponding Lamb shift components are listed in Table II. The Uehling vacuum polarization and black-hole-exchange model Lamb shift components differ by ~0.1%. The convergence of the presented black-hole exchange model towards Uehling is highlighted in Fig. 18. Only by including the correlated exchanges (black hole clusters), can the correct force be obtained at short length scales at $r < 1$. The number of particle units per cluster grows logarithmically as the distance between the exchanging pair goes to zero. This has similarities to standard QED where the high electric fields as r approaches zero are maintained by the coordinated effort of a large number of virtual electron-positron pairs.

IX.D Vacuum polarization summary

The combination of simple terms in Eq. (57) accurately mimics the properties of vacuum polarization. This could be an example of an apparent explanation (or fit) by including a number of simple assumptions that were chosen, in part, because of the corresponding favorable outcomes. These assumptions are:

(1) In a similar fashion to photon exchanges, there is a force between two closely spaced real electrons due to the exchange of virtual single black holes ($s = 1/2$ electrons) given by Eq. (54). There are five assumptions that transform the photon exchange force into Eq. (54): (a) a sign changes due to the Boson to Fermion exchange switch; (b) the exponential reduction factor associated with the rest-mass of the exchanging particle; (c) near-field effects are calculated using a wavelength $\lambda\!\!\!^{-}_0 = \hbar c/\varepsilon$, where ε is the energy of the exchanging particle in excess of its rest-mass energy; (d) a factor of two due to the system not being able to track which black hole is the parent and which is the evaporated daughter; and (e) the estimation of a transmission coefficient using an effective barrier radius of $2\alpha d/\pi$. These modifications are partially justified by a comparison of this picture with standard vacuum polarization at distances $d > \lambda\!\!\!^{-}_C$ (see Fig. 24); and

(2) There is a force between two closely spaced real electrons associated with the exchange of virtual clusters of j black holes (electrons). To deal with these multiple-particle exchanges, only three additional assumptions are needed: (a) even j clusters behave as $s = 1$ Bosons with only two states of helicity (like photons), while odd j clusters are considered $s = 1/2$ Fermions; (b) there is a reduction factor of $1/j$ associated with cluster evaporation; and (c) a further reduction factor of $1-1/2\pi$ for Boson evaporation, associated with these emissions having a self-absorption probability of $1/2\pi$. These modifications are partially justified by their ability, in conjunction with (1), to closely match the properties of vacuum polarization down to distances much smaller than $\lambda\!\!\!^{-}_C$, and give Lamb shift components that differ from those due to Uehling vacuum polarization by less than a relative change of α/π.

A summary of several estimates of relative potential changes due to vacuum polarization is presented in Fig. 27. The dotted curve is the standard vacuum polarization result from Uehling, and the dash-dotted and dash-double-dotted curves are the corresponding large and small length scale limits as given by Eq.s (45) and (46). The dashed curve is our result from the presented virtual black hole and virtual black-hole cluster exchange model. Its ability to follow the standard vacuum polarization result over ten orders of magnitude in relative potential change, across four orders of magnitude in distance, is stunning. The agreement is at a level of $\sim\alpha/\pi$ in the region of r = 0.05 to 7. This level of agreement deteriorates slowly as we move to smaller and larger length scales but is still only a few percent at the edges of Fig. 27. The

ability to expand on the photon exchange concept and obtain a new picture of vacuum polarization adds some credibility to the assumptions used to obtain estimates of the fine-structure constant in section VII.

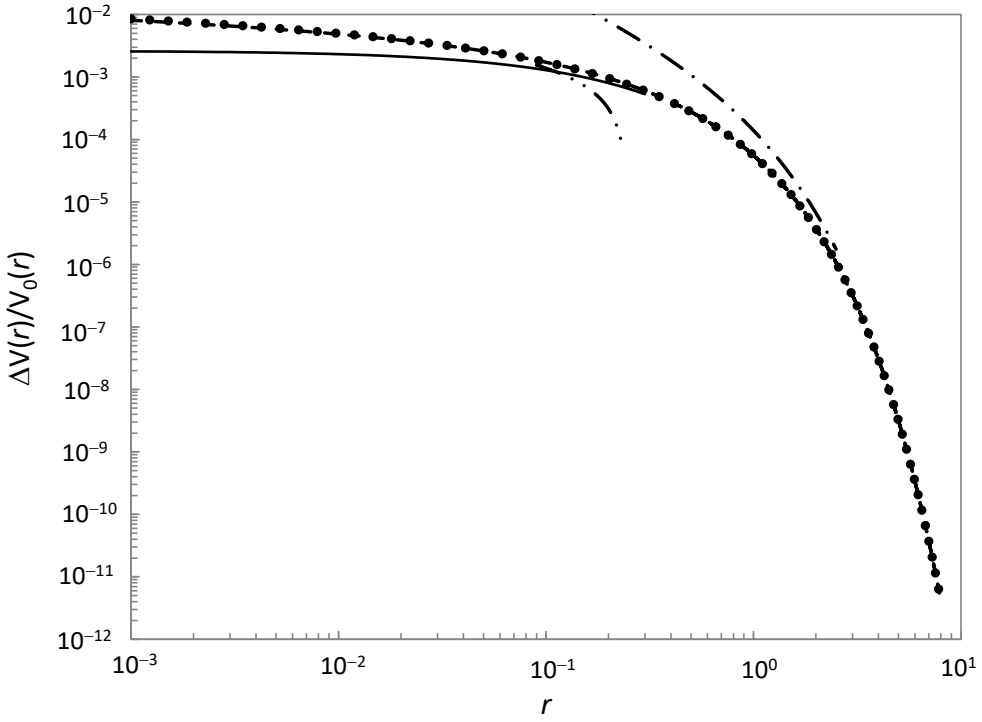

Fig. 27. Various estimates of relative potential changes due to vacuum polarization: the vacuum polarization result of Uehling (dotted curve which may be difficult to see because it coincides with the dashed curve); the corresponding large and small length scale approximations (dash-dotted and dash-double-dotted curves); and the result from the present virtual black hole and virtual black-hole cluster exchange model (dashed curve). The solid curve shows the corresponding result with the exchange of only virtual single black holes (i.e. without any cluster exchanges).

Ignoring the possibility of a fortuitous result via many selective model choices, the results presented here suggest vacuum polarization might be mappable into the exchange of virtual single black holes (electrons) and virtual black-hole clusters between interacting real particles. At first, it might appear as though the proposed new picture has little in common with the standard view. However, on a closer look, perhaps the new picture is not that dissimilar. In the standard picture, virtual electron and positron pairs are polarized with the virtual electrons pushed away from a central negative charge, while the virtual positrons are pulled inwards. Therefore, if one imagines a sphere around an electron at a distance d then there will be an outward flux of virtual electrons through this sphere. In the case of an isolated (single) electron, the outward flux would be balanced by the inward flux of returning virtual electrons that need to annihilate with the virtual positrons. The size of the outward going virtual-electron flux will increase with decreasing d. In the case of an interacting real electron pair, virtual electrons moving away from one of the real electrons might annihilate with a virtual positron near the partner real electron. This exchange of a virtual electron can be viewed as evaporation from one of the real electrons and absorption by the corresponding nearby real partner as depicted in Fig. 28(a). At $d > \lambda\!\!\!^{-}_C$, one might expect the outward going electrons from a single real particle to be rare and relatively independent of other emissions. At smaller length scales, correlations in the outgoing electron flux would be expected, with these correlations increasing with decreasing d. The cylindrical structures (tubes) in Fig. 28 are an attempt to acknowledge that on short length scales real particles are intrinsically fuzzy objects containing a surrounding sea of virtual photons and particles. We suggest this sea has thermal-like properties, and can evaporate and

absorb virtual electrons and complex electron clusters in a manner that is similar to other hot objects. In Fig. 28(a) we see that the depicted exchange cannot be completed unless there is some type of coordination between the remaining unpaired electron and positron. If this leftover pair finds each other, we obtain Fig. 28(b). This is the QED one-loop vacuum polarization diagram. Perhaps processes like these are being partially mimicked by Eq. (57). In the standard picture of vacuum polarization, the high electric fields at $r << 1$ are maintained by the coordinated effort of multiple virtual electron-position pairs. This may be paralleled in the new picture where the force at short length scales is generated by the exchange of correlated black holes (electrons) in clusters.

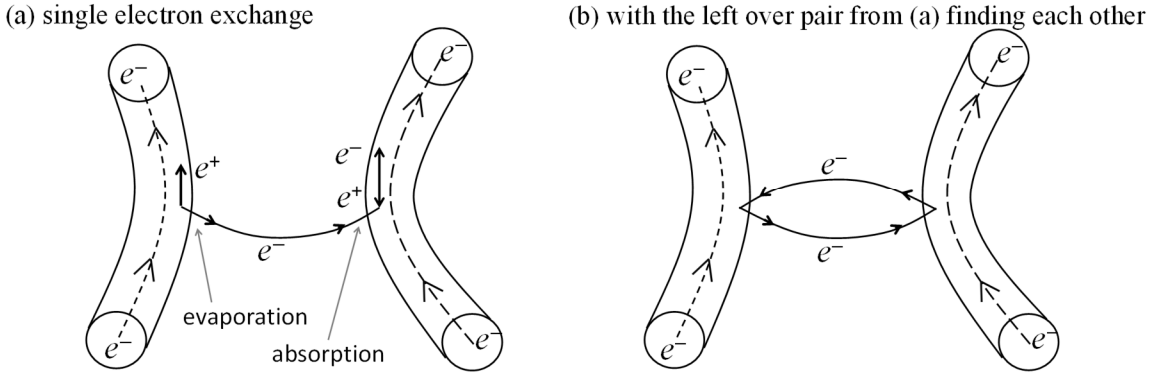

Fig. 28. (a) A depiction of a single electron exchange between two real electrons. (b) We force the leftover (spare) electron-positron pair from (a) to find each other, thus forming an electron loop. The cylindrical structures (tubes) acknowledge that at short length scales real electrons are intrinsically fuzzy objects which contain a complex sea of virtual photons and particles.

X. Summary

By assuming that vacuum-virtual photons can stimulate an isolated small black hole to emit additional virtual photons with a cross section of $\pi\lambda\!\!\!^{-2}$, and invoking a high-energy cutoff of $2\pi mc^2$ beyond which vacuum-virtual photons no longer interact with the particle, the additional energy associated with the cloud of stimulated-virtual photons surrounding a massless particle is on average equal to mc^2. This virtual photon emission mechanism is essentially the same as Hawking radiation but for $L = 0$ unphysical photon emission instead of $L > 0$ real emission. The storage of the rest energy in the surrounding cloud of virtual photons is similar to the storage of the rest energy in the surrounding classical electric field, but without the infinities associated with classical point particles. The high-energy cutoff of $2\pi mc^2$, in conjunction with the semi-classical low-energy Lamb-shift cutoff of $\sim\alpha mc^2$ [17] and an absorption (with recoil) cross section of $\alpha\pi\lambda\!\!\!^{-2}$, leads to a calculated hydrogen Lamb shift of ~1000 MHz. This apparent success supports the idea that photon-electron interaction cross sections of $\pi\lambda\!\!\!^{-2}$ and $\alpha\pi\lambda\!\!\!^{-2}$ play an important role in QED processes. The inclusion of near-field effects and other model choices gives the anomalous magnetic moment of the free electron. These choices are partially justified by their ability to give the correct $(\alpha Z)^2$ dependence of the magnetic moment of electrons in hydrogen-like atoms with the assumed self-interaction high-energy cutoff of $\varepsilon_S = \pi\hbar c/d$.

An expression for the fine-structure constant can be obtained if electromagnetism is assumed to be associated with the exchange of stimulated-virtual photons between particle pairs. Including estimates of near-field effects that give the electron's magnetism, and direction-reversing stimulated emission inspired by the calculated properties of black holes by others [15], leads to a force between particles that defines a fundamental unit of charge of $(1.601\pm0.002)\times10^{-19}$ C with a corresponding fine-structure constant of $\alpha =$

1/(137.18±0.32). Additional, but more speculative assumptions about higher-order corrections, give an inverse fine-structure constant α^{-1} = 137.06±0.02 with a fundamental unit of charge of (1.6020±0.0002)×10^{-19} C. A minor modification in the way that direction-reversed stimulated photons interact with accelerating electrons gives a new picture of Larmor emission that does not require a radiation resistance.

An expansion on the force generated by the exchange of virtual photons to include the exchange of virtual electrons gives a new picture of vacuum polarization. This picture contains multiple plausibility arguments based on intuition obtained via the study of evaporation and absorption by other hot objects. Applying these concepts to vacuum polarization is highly unorthodox. However, the level of agreement between Uehling and the presented model shown in Fig. 27 suggests additional investigations into the use of thermal-like evaporation to mimic QED processes is warranted. If the presented course of action turns out to be fruitful then the connection between electromagnetism and the statistical theory of particle evaporation and absorption is likely to lead to additional findings.

The closeness of the presented model calculations to experiment and standard QED theory does not prove the model choices made here are correct because in many cases these choices are based on the favorable outcomes generated. The main testable outcomes from the present study are the suggestions that:

(1) The rest energy of very small chargeless black holes is due to stimulated-virtual photon emission generated by the interaction of these black holes with virtual photons associated with the electromagnetic vacuum. This interaction has a high-energy cutoff of unknown origin.

(2) The above interaction is divided into two components. The dominant part is a relatively simple interaction whose only outcome is the above-discussed stimulated-virtual photon emission. A component ~137 times weaker than the dominant interaction generates a short time movement or blurring of the black hole by a length scale of ~ $\lambda\!\!\!^{-}_C$.

(3) For stimulated-virtual photons born a finite distance d, from a future interaction location, near-field effects reduce the above-discussed interactions by a factor of $1-\exp(-2d^2/\pi\lambda\!\!\!^{-2})$, with these interactions having a high-energy cutoff of $\pi\hbar c/d$.

(4) Virtual black holes in the presence of a pair of real charged particles separated by a distance d, must be separated from the real particles by a distance larger than $2\alpha d/\pi$ before they can be viewed by the electromagnetic vacuum as a separate entity.

It is possible that these suggestions could be tested by a detailed theoretical study of the interaction of photons with small black holes and black hole pairs. The long wavelength exchange of Hawking radiation between a pair of black holes will be of particular interest.

Given the results presented here, we feel that we cannot currently dismiss the possibility that the fine-structure constant and several other QED results are obtainable via a far-field photon-electron interaction cross section of $\pi\lambda\!\!\!^{-2}$ with near-field effects and direction-reversed stimulated emission. A summary of our reverse-engineered semi-classical results is presented in Table III and Fig. 29. Additional work on photon-particle near-field effects, direction-reversing stimulated emission, black-hole-electron interactions, and higher-order effects is needed to confirm or negate the semi-classical suggestions made here. If the semi-classical choices made here can be justified by detailed calculations, then an understanding of the numerical value of the fine-structure constant may emerge. Despite the speculative nature of several of the arguments used to obtain a calculated value near to the known fine-structure constant, the present study suggests that charge is an emergent property generated by a simple interaction mechanism between point-like chargeless particles (black holes) and the vacuum state.

Table III. Summary of the semi-classical results obtained here, and a comparison with QED.

Observable	Simple semi-classical results		QED
	Reason	Formula	
Rest energy	Emission and self-absorption of stimulated-virtual photons	$E = \int_0^{2\pi mc^2} \int_0^{\infty} \frac{2\varepsilon^2}{\pi\hbar^2} t \exp(-2\varepsilon t/\hbar)\, dt\, d\varepsilon = mc^2$	
Lamb shift (excluding vacuum polarization and the shift of the *p* state)	Absorption and re-emission of vacuum-virtual photons	$\Delta E_{2s} \sim \frac{\alpha^5 \ln(2\pi/\alpha)}{6\pi} mc^2$ ~1000 MHz	1072 MHz
Anomalous magnetic moment of the free electron	Stimulated emission and self-interaction including near-field effects, following the absorption and re-emission of vacuum-virtual photons	$\frac{(g-2)}{2} = \frac{\alpha}{2\pi}$ (second order)	$\frac{\alpha}{2\pi}$ (second order)
Magnetic moment of the electron in hydrogen-like atoms	Stimulated emission and self-interaction including near-field effects and system size	$\frac{\mu_e(1s)}{\mu_B} \sim 1 + \frac{\alpha}{2\pi} - \frac{\alpha^2 Z^2}{3}\left(1 - \frac{2m}{M}\right)$	$1 + \frac{\alpha}{2\pi} - \frac{\alpha^2 Z^2}{3}\left(1 - \frac{3m}{2M}\right)$
Fine-structure constant	Exchange of stimulated-virtual photons including near-field effects and time-reversing stimulated emission	$\alpha = \frac{1+\alpha/2\pi}{2\pi} \int_0^{2\pi} \frac{[1-\exp(-\varepsilon^2/2\pi)]^2}{\exp(\varepsilon) - 1 + (1 \pm 1)\alpha/2\pi} \frac{d\varepsilon}{\varepsilon}$ α = 1/137.06(2)	~1/137.035999206(11) (experiment)
Larmor emission	Modification to the interaction of direction-reversed emission due to particle acceleration	$P = \frac{a^2\hbar}{c^2} \frac{2}{\pi} \frac{1+\alpha/2\pi}{1+4\alpha} \int_0^{2\pi} \frac{\{1-\exp(-\varepsilon^2/2\pi)\}^2 \exp(-\varepsilon)}{\exp(\varepsilon) - 1 + (1 \pm 1)\alpha/2\pi} \frac{d\varepsilon}{\varepsilon}$ $= 0.6666(2) \cdot \alpha a^2 \frac{\hbar}{c^2}$	$\frac{2}{3} \cdot \alpha a^2 \frac{\hbar}{c^2}$
Vacuum polarization	Including virtual electron exchanges	See Eq. (57)	See Fig. 27 and Table II

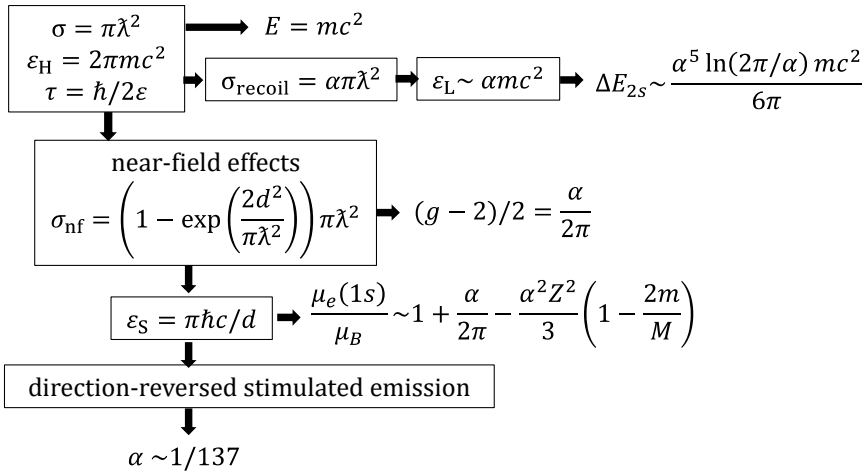

Fig. 29. Summary of the connection between assumptions (rectangles) and results leading to a numerical estimate of the fine-structure constant.

Appendix A. Some key proofs related to the Larmor emission section

The mathematics required to follow the presented work is of a rather elementary level compared to the needs for understanding standard QED. However, the algebra for a few of the Larmor emission proofs is a little tedious. To facilitate the reader through the more tedious algebra, a few of the proofs are presented here in greater detail.

As per Fig. 15 we assume a stationary but accelerating electron initiates an exchange with a stationary massive particle of unit charge at a distance d_0. This initial exchange takes a time $t_1=d_0/c$ to complete. In this time, the electron is displaced by $at_1^2/2$, and thus at t_1 the massive-particle-to-electron separation distance is $d_1=d_0(1+ad_0/(2c^2))$. After t_1 the electron's location is given by $d(t)=d_1+v_1t+at^2/2$, where here t is the elapsed time after t_1, and $v_1=at_1=ad_0/c$. At t_1, a direction-reversed photon is sent back from the massive particle towards the electron. We define t_2 to be the time at the completion of this second exchange relative to the time of initiation of the first exchange. The time to complete the second exchange $\Delta t=t_2-t_1$ can be obtained by solving $d_2(\Delta t)=c\Delta t=d_1+v_1\Delta t+a\Delta t^2/2$, i.e. $0=(a/2)\Delta t^2+(v_1-c)\Delta t+d_1$. The corresponding solution is

$$\begin{aligned}
\Delta t &= \left(\frac{c-v_1}{a}\right)-\sqrt{\frac{(c-v_1)^2-2ad_1}{a^2}}=\left(\frac{c-v_1}{a}\right)\left\{1-\sqrt{1-\frac{2ad_1}{c^2+v_1^2-2cv_1}}\right\}\\
&=\left(\frac{c-v_1}{a}\right)\left\{1-\sqrt{1-\frac{2ad_1}{c^2}\frac{1}{1-\frac{2ad_0}{c^2}+\left(\frac{ad_0}{c^2}\right)^2}}\right\}\\
&=\left(\frac{c-v_1}{a}\right)\left\{1-\sqrt{1-\frac{2ad_1}{c^2}(1-(-2\beta+\beta^2)+(-2\beta+\beta^2)^2-\cdots)}\right\}\ \text{where } \beta=ad_0/c^2\\
&=\left(\frac{c-v_1}{a}\right)\left\{1-\sqrt{1-\frac{2ad_1}{c^2}(1+2\beta+3\beta^2+\cdots)}\right\}\\
&=\left(\frac{c-v_1}{a}\right)\left\{1-\sqrt{1-\frac{2ad_0(1+\beta/2)}{c^2}(1+2\beta+3\beta^2+\cdots)}\right\}\\
&=\left(\frac{c-v_1}{a}\right)\left\{1-\sqrt{1-2\beta-5\beta^2-8\beta^3-\cdots}\right\}\\
&=\left(\frac{c-\beta c}{a}\right)\left\{1-\left(1-\frac{1}{2}(2\beta+5\beta^2+8\beta^3)-\frac{1}{8}(2\beta+5\beta^2+\cdots)^2-\frac{1}{16}(2\beta+\cdots)^3-\cdots\right)\right\}\\
&=\frac{c}{a}(1-\beta)(\beta+3\beta^2+7\beta^3+\cdots)\\
&=\frac{c}{a}(\beta+2\beta^2+4\beta^3+\cdots)=\frac{d_0}{c}(1+2\beta+4\beta^2+\cdots)
\end{aligned}\tag{36}$$

and therefore

$$\begin{aligned}
d_2 &= c\Delta t=d_0(1+2\beta+4\beta^2+\cdots)\\
d_2^2 &= d_0^2(1+2\beta+4\beta^2+\cdots)^2=d_0^2(1+4\beta+12\beta^2+\cdots)\\
\left(\frac{d_0}{d_2}\right)^2 &= \frac{1}{1+4\beta+12\beta^2+\cdots}=1-(4\beta+12\beta^2+\cdots)+(4\beta+12\beta^2+\cdots)^2-\cdots\\
&=1-4\beta+4\beta^2.
\end{aligned}\tag{37}$$

In the case of an accelerating electron, at the time of the reabsorption of the double exchange by the electron, the electron will have a velocity v_2, away from the massive stationary particle. The frequency f_2 of the reabsorbed photon, as seen (observed) by the reabsorbing electron, will be Doppler shifted to a lower value than the frequency as seen by the source f_0 with

$$f_2=f_0\frac{1}{1+\frac{v_2}{c}}\cdot\frac{1}{\sqrt{1-\left(\frac{v_2}{c}\right)^2}}=f_0\left\{1-\frac{v_2}{c}+\left(\frac{v_2}{c}\right)^2-\cdots\right\}\cdot\sqrt{1+\left(\frac{v_2}{c}\right)^2+\left(\frac{v_2}{c}\right)^4+\cdots}$$

$$= f_0\left\{1-\frac{v_2}{c}+\left(\frac{v_2}{c}\right)^2-\cdots\right\}\cdot\left\{1+\frac{1}{2}\left(\frac{v_2}{c}\right)^2+\cdots\right\}$$
$$= f_0\left\{1-\frac{v_2}{c}+\frac{3}{2}\left(\frac{v_2}{c}\right)^2+\cdots\right\}$$

The velocity v_2 is given by $v_1+a\Delta t$, and with the results obtained above we get

$$v_2 = \frac{ad_0}{c}+\frac{ad_0}{c}(1+2\beta+4\beta^2+\cdots) = c(2\beta+2\beta^2+\cdots) \text{ and thus}$$
$$f_2 = f_0\left\{1-(2\beta+2\beta^2+\cdots)+\frac{3}{2}(2\beta+2\beta^2+\cdots)^2+\cdots\right\} = f_0\{1-2\beta+4\beta^2+\cdots\}$$
$$f_2^2 = f_0^2\{1-4\beta+12\beta^2+\cdots\}$$
$$\left(\frac{\lambda_2}{\lambda_0}\right)^2 = \frac{1}{1-4\beta+12\beta^2+\cdots} = 1-(-4\beta+12\beta^2+\cdots)+(-4\beta+12\beta^2+\cdots)^2$$
$$= 1+4\beta+4\beta^2+\cdots \quad (38)$$

The effective size of the photon-electron interaction is modified by the electron's acceleration by the factor

$$\left(\frac{d_0}{d_2}\frac{\lambda_2}{\lambda_0}\right)^2 = (1-4\beta+4\beta^2+\cdots)(1+4\beta+4\beta^2+\cdots)$$
$$= 1+4\beta+4\beta^2+\cdots-4\beta-16\beta^2+\cdots+4\beta^2+\cdots$$
$$= 1-8\beta^2+\cdots\ . \quad (39)$$

References

[1] S. Tomonaga, Prog. Theor. Phys. **1**, 27 (1946).
[2] J. Schwinger, Phys. Rev. **73**, 416 (1948); **74**, 1439 (1949); **76**, 790 (1949).
[3] R. P. Feynman, Phys. Rev. **76**, 749 (1949); **76**, 769 (1949).
[4] Mohr, P.J.; Taylor, B.N.; Newell, D.B. 2018 CODAT recommended values. National Institute of Standards and Technology. Gaithersburg, MD: U.S. Department of Commerce.
[5] L. Morel et al, Nature **588**, 61 (2020).
[6] U. D. Jentschura and I. Nandori, Eur. Phys. J. H, **39**, 591 (2014).
[7] S. W. Hawking, Nature **248**, 30 (1974).
[8] C. F. E. Holzhey and F. Wilczek, Nucl. Phys. B **380**, 447 (1992).
[9] B. Carter, Phys. Rev. **174**, 1559 (1968).
[10] A. Einstein, L. Infeld, and B. Hoffmann, Ann. Math. **39**, 65 (1938).
[11] J. P. Lestone, arXiv:physics/0703151, v1 (2007).
[12] R. Fabbri, Phys. Rev. D **12**, 933 (1975).
[13] D. N. Page, Phys. Rev. D **13**, 198 (1976).
[14] L. C. B. Crispino, E. S. Oliveira, A. Higuchi, and G. E. A. Matsas, Phys. Rev. D **75**, 104012-1 (2007).
[15] J. D. Bekenstein and A. Meisels, Phys. Rev. D **15**, 2775 (1977).
[16] J. P. Lestone, Mod. Phys. Lett. A **23**, 1067 (2008).
[17] J. D. Bjorken and S. D. Drell, Relativistic Quantum Mechanics, McGraw-Hill ISBN 07-005493-2 (1964).
[18] F. Wilczek, Inter. Journ. of Modern Phys. A. **13**, 5279 (1998).
[19] E. A. Uehling, Phys. Rev. **48**, 55 (1935).
[20] W. E. Lamb and R. C. Retherford, Phys. Rev. **72**, 241 (1947).
[21] H. A. Bethe, Phys. Rev. **72**, 339 (1947).
[22] S. G. Karshenboim, Can. J. Phys. **76**, 168 (1998).
[23] T. Kinoshita, and M. Nio, Phys. Rev. D **73**, 053007 (2006).

[24] T. A. Welton, Phys. Rev. **74**, 1157 (1948).
[25] Z. Irahhauten et al., IEEE International Conference on Communication, 2008, pg. 4872.
[26] H. Grotch, Phys. Rev. Lett. **24**, 39 (1970).
[27] J. S. Tiedeman and H. G. Robinson, Phys. Rev. Lett. **39**, 602 (1977).
[28] H. Grotch, Phys. Rev. A **2**, 1605 (1970).
[29] S. G. Karshenboim, arXiv:hep-ph/0008227 (2000).
[30] F. G. Walther, W. D. Phillips and D. Kleppner, Phys. Rev. Lett. **28**, 1159 (1972).
[31] D. J. Larson and N. F. Ramsey, Phys. Rev. A **9**, 1543 (1974).
[32] C. E. Johnson and H. G. Robinson, Phys. Rev. Lett. **45**, 250 (1980).
[33] T. Beier et al, Nucl. Inst. Meth. B **205**, 15 (2003).
[34] A. Petermann, Helv. Phys. Acta, 30, 407 (1957).
[35] S. Laporta and E. Remiddi, Phys. Lett. B, 379, 283 (1996).
[36] R. P. Feynman, R. B. Leighton, and M. Sands, The Feynman Lectures on Physics, volume II, section 28 (1964).
[37] K. Pachucki, Phys. Rev. A **60**, 3593 (1999).
[38] A.A. Krutov and A. P. Martynenko, Phys. Rev. A **84**, 052514 (2011).
[39] S. Iso, H. Umetsu, and F. Wilczek, Phys. Rev. Lett. **96**, 151392 (2006)
[40] M. K. Parikh and F. Wilczek, Phys. Rev. Lett. **85**, 5042 (2000)
[41] R. Kerner and R. B. Mann, Phys. Lett. B **665**, 227 (2008).
[42] J. P. Lestone and S. G. McCalla, arxiv:0807.3362 (2008).
[43] J. P. Lestone, Intern. Journ. of Mod. Phys. E **17**, 323 (2008).
[44] R. Hanbury Brown and R. Q. Twiss, Nature **177**, 27 (1956).
[45] R. Hanbury Brown and R. Q. Twiss, Nature **178**, 1046 (1956).